Theoretical and Computational Fluid Dynamics (2013) 27(6):735–766
(the final publication is available at `link.springer.com/article/10.1007/s00162-012-0266-x`)

B. Scheichl · A. Kluwick

Non-unique turbulent boundary layer flows having a moderately large velocity defect

A rational extension of the classical asymptotic theory

Received: 19 October 2011 / Accepted: 22 March 2012 / Published online: 26 April 2012

Abstract The classical analysis of turbulent boundary layers in the limit of large Reynolds number *Re* is characterised by an asymptotically small velocity defect with respect to the external irrotational flow. As an extension of the classical theory, it is shown in the present work that the defect may become moderately large and, in the most general case, independent of *Re* but still remain small compared to the external streamwise velocity for non-zero pressure gradient boundary layers. That wake-type flow turns out to be characterised by large values of the Rotta–Clauser parameter, serving as an appropriate measure for the defect and hence as a second perturbation parameter besides *Re*. Most important, it is demonstrated that also this case can be addressed by rigorous asymptotic analysis, which is essentially independent of the choice of a specific Reynolds stress closure. As a salient result of this procedure, transition from the classical small-defect to a pronounced wake flow is found to be accompanied by quasi-equilibrium flow, described by a distinguished limit that involves the wall shear stress. This situation is associated with double-valued solutions of the boundary layer equations and an unconventional weak *Re*-dependence of the external bulk flow – a phenomenon seen to agree well with previous semi-empirical studies and early experimental observations. Numerical computations of the boundary layer flow for various values of *Re* reproduce these analytical findings with satisfactory agreement.

Keywords Matched asymptotic expansions · Boundary layer theory · Turbulence

PACS 45.10.Hj · 47.27.Jv · 47.27.Nz

1 Motivation and introduction

We initiate the present investigation by a critical review of the current knowledge gained in the course of preceding asymptotic studies of turbulent boundary layers. This leaves its mark on a conceptual flow description which can be exploited rigorously.

B. Scheichl (Corresponding Author)
AC²T research GmbH (Austrian Center of Competence for Tribology), Viktor-Kaplan-Straße 2, A-2700 Wiener Neustadt, Austria
and
Institute of Fluid Mechanics and Heat Transfer, Vienna University of Technology, Resselgasse 3/E322, A-1040 Vienna, Austria
Tel.: +43-1-58801-322-25
E-mail: bernhard.scheichl@tuwien.ac.at

A. Kluwick
Institute of Fluid Mechanics and Heat Transfer, Vienna University of Technology, Resselgasse 3/E322, A-1040 Vienna, Austria
Tel.: +43-1-58801-322-20
E-mail: alfred.kluwick@tuwien.ac.at

1.1 Basic physical concept

A rational theory of incompressible wall-bounded turbulent shear flows past a smooth surface in the large-Reynolds-number limit on basis of the full set of the time- or, equivalently, Reynolds-averaged Navier–Stokes equations governing the fluid mean motion has been formulated first in the pioneering papers of Yajnik [1], Bush & Fendell [2], Fendell [3], and Mellor [4], and surveyed more recently together with further developments by Walker [5] and Gersten in the textbook by Schlichting & Gersten [6]. Basically, their approach formalises the well-established results obtained by means of intuitive and dimensional reasoning in the early seminal studies by Theodor von Kármán and Ludwig Prandtl. Here [6] represents a definite reference. In a further contribution indisputably worth mentionable in this respect, Deriat & Guiraud [7] considered the averaging process and the underlying cascade of length and time scales in more depth and breadth, but to some extent by inheriting the ideas of scaling as given in the above studies. Conversely, the analysis in [7] lends also support to the very structure of the Reynolds-averaged flow typically associated with those.

That hereafter termed "classical" asymptotic theory of turbulent boundary layers is initially guided by the empirical observation that, in the here presumed absence of free-stream turbulence, the turbulent motion is essentially confined to a thin shear layer adjacent to the surface under consideration, which *per se* gives rise to the definition of a boundary layer. Furthermore, it deals with fully developed turbulence only. That is, it describes boundary layers which are characterised by a fully turbulent outer main part, adjoining the external free-stream flow and comprising most of the boundary layer, where the Reynolds stresses predominate over the viscous ones. This idea of a turbulent boundary layer then implies two consequences which are very important from a theoretical point of view: Firstly, it states that the turbulent velocity and pressure fluctuations are considered to be (asymptotically) small compared to their time-mean counterparts, at least outside of the near-wall flow regime. In turn, the Reynolds stresses are taken to be accordingly small, too. Secondly, in view of the usual no-slip condition holding at the surface it predicts the existence of a sublayer adjoining to the surface, the so-called viscous wall layer, where the molecular stresses and their turbulent counterparts are of comparable magnitude.

The qualitative concept outlined so far provides a widely accepted framework for the time-mean description of the boundary layer flow. Moreover, it subsequently turns out to prove extraordinarily fruitful for establishing a most general theory of turbulent boundary layers which shall be based on a minimum of postulates regarding the nature of turbulent momentum exchange for arbitrarily high Reynolds numbers.

As the primary consequence of the above considerations, the classical theory applies to firmly attached boundary layers only as it essentially employs the principal assumption of a small (mean) streamwise velocity defect holding in the fully turbulent main region of the shear layer. This stipulation is motivated by scaling arguments but also the conclusion that the no-slip condition is not met necessarily at the base of the outer main flow regime as there the aforementioned viscous wall region is regnant (and the small defect on its top prevents the pressure gradient from effectively influencing the predominant shear stress equilibrium). As a matter of fact, however, the concept of an asymptotically small velocity defect adopts a different assumption we assign the status of a basic hypothesis. To be more precise, the latter can be cast in the following form:

Hypothesis 1 (classical) *In the high-Reynolds-number limit in the Reynolds-averaged equations of motion the turbulent dynamics outside the viscous near-wall region is represented by a single velocity scale.*

In other words, that means that the turbulent velocity scale is uniquely determined by the magnitude of the Reynolds shear stress which, as the asymptotic analysis shows, originates from a match with the viscous near-wall region. Physically, that statement seems viable as it is the strongly viscosity-affected near-wall flow regime which emits turbulent motion into the outer part of the boundary layer in order to maintain self-sustained turbulence. As a constitutive property of turbulent shear flows accounted for in the classical approach, both the turbulent fluctuations and the shear layer thickness then are believed to vanish in the limit of infinite Reynolds number.

It is, however, the main purpose of the present investigation to extend the classical theory by relaxing Hypothesis 1 and then, in combination with the (rather plausible) basic assumptions outlined above and elaborated below, adopting strictly rigorous asymptotic techniques in order to devise a more general fully self-consistent flow description. That weaker generalised version of Hypothesis 1 is formulated as follows:

Hypothesis 2 (relaxed or generalised) *In the high-Reynolds-number limit in the Reynolds-averaged equations of motion the turbulent dynamics outside the viscous near-wall region is represented* locally *by a single velocity scale (which then may vary with distance normal to the wall).*

Although sounding rather unspecified at first, this premise provides the firm basis for a fundamental and capacious asymptotic concept: it predicts a multi-layered splitting of the boundary layer as a consequence of the various velocity scales acting at respective disparate length scales. Thus it dictates the use of matched asymptotic expansions as the proper tool for a theoretical investigation. Nevertheless, it includes Hypothesis 1 and, thus, the classical structure as a special case. We remark, however, that the authors also intend to carefully analyse the general Hypothesis 2 on basis of the full set of Navier–Stokes equations in a separate study. Also, it is noted that both the hypotheses stated above include the assumption that all components of the Reynolds stress tensor are equally scaled in the limit of arbitrarily large Reynolds number. This is employed tacitly throughout in the following and equivalent to the commonly adopted hypothesis of locally isotropic turbulence in the sense of Kolmogorov: see [8] and the references therein, Hinze [9], pp. 175–177, and Monin & Yaglom [10]. An even more relaxed form of Hypothesis 2 was already adopted by the authors: see the survey paper by Kluwick & Scheichl [11] and the related references cited there. It additionally allows for a large velocity defect accounting for marginally separated flows, with the velocity scale determining the Reynolds stresses being small though. However, for initially attached flow the celebrated logarithmic law of the wall then is presumed rather than purely a consequence of the matching procedure, as it appears due to the present formulation.

This paper is organised as follows: in Subsect. 1.2 all the remaining prerequisites made and the basic equations forming the problem of the time-averaged flow are formulated. In Sect. 2 both the Hypotheses 1 and 2 are exploited, i.e. restated in a more formal manner, for devising the asymptotic structure of the flow. The description of the fully turbulent flow regime based on the generalised asymptotic concept, capturing the difference to the classical scaling of the flow, is envisaged in detail in Sect. 3. The comparison with existing measurements proves satisfactory. Here the prediction of double-valued equilibrium flows for a given external pressure gradient marks a highlight, prompted by a digression on the route to turbulence in the neighbourhood of their virtual origin. In Sect. 4 these asymptotic results are compared with suitable experimental data (available in the literature) and those obtained by numerical integration of the full boundary layer equations, which then are parametrised by the Reynolds number.

1.2 Problem formulation and governing equations

We consider an incompressible nominally steady and two-dimensional fully developed turbulent boundary layer along a smooth and impermeable solid surface, being e.g. part of a diffuser duct. All flow quantities are non-dimensional with respect to a reference velocity $\tilde{U}$ which characterises the magnitude of the bulk flow, a reference length $\tilde{L}$, characteristic of the variation of the flow in mean flow direction (and also the wall contour), and the uniform fluid density. Together with the constant kinematic fluid viscosity $\tilde{\nu}$ these quantities then suitably define a global Reynolds number Re, which is taken to be large:

$$Re = \tilde{U}\tilde{L}/\tilde{\nu} \to \infty. \tag{1}$$

The flow configuration is sketched in Fig. 1 (a): Let x, y, u, v, and p denote curvilinear coordinates, respectively, along and perpendicular to the surface, where the latter is given by $y = 0$, the streamwise and normal time-mean velocity components, and the time-mean gauge pressure with respect to its value in the fluid at rest. The surface curvature $k(x)$ is assumed to be a quantity of $O(1)$. Furthermore, a relatively thin overlayer has to be distinguished in principle which accounts for the intermittent but rather sharp free-stream boundary of turbulent shear layers. However, since it would not affect the subsequent analysis substantially, it is disregarded here. That is, here a distinct outer edge of the boundary layer is assumed to be observed a distance $y = \delta(x;Re)$ from the wall. Both the variation of the boundary layer thickness δ with x and its asymptotic dependence on Re are *a priori* unknown. We, therefore, first only impose the weak requirement

$$\delta(x;Re) \ll 1 \quad \text{as} \quad Re \to \infty. \tag{2}$$

This relationship expresses that turbulence essentially takes place within a thin wall-bounded shear layer. In the formal limit $\delta \to 0$ the streamwise velocity u there then asymptotically equals the surface slip velocity imposed by the external bulk flow, which in the following is referred to as $U_e(x)$.

It is expedient to introduce a stream function ψ by

$$\partial\psi/\partial y = u, \;\; \partial\psi/\partial x = -hv, \quad h = 1 + k(x)y, \tag{3a}$$

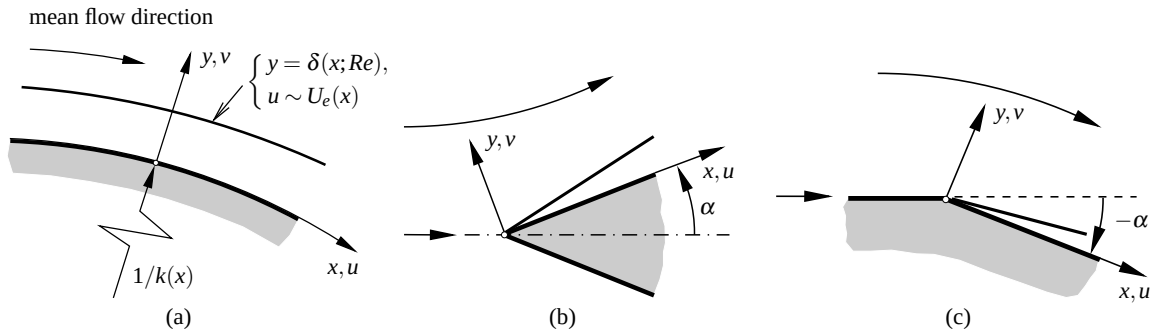

Fig. 1 (a) Flow configuration using a natural coordinate system, here shown for a positive (convex) surface curvature $k(x)$ (radius $1/k(x)$ of curvature), specified for (b) a symmetric wedge-type potential flow (wedge angle 2α), (c) a convex-corner-type potential flow (negative wedge angle α)

so that the continuity equation is satisfied identically. Adopting the common notation for the turbulent stresses, where the primes denote the turbulent fluctuations of the corresponding velocity components, we write the dimensionless Reynolds-averaged equations of motion in the form

$$h\Big(\frac{\partial\psi}{\partial y}\frac{\partial}{\partial x}-\frac{\partial\psi}{\partial x}\frac{\partial}{\partial y}\Big)\frac{\partial\psi}{\partial y}-k\frac{\partial\psi}{\partial x}\frac{\partial\psi}{\partial y}=-h\frac{\partial p}{\partial x}-h\frac{\partial\langle u'^2\rangle}{\partial x}-\frac{\partial h^2\langle u'v'\rangle}{\partial y}+\frac{h^2}{Re}\frac{\partial\nabla^2\psi}{\partial y}, \tag{3b}$$

$$\Big(\frac{\partial\psi}{\partial x}\frac{\partial}{\partial y}-\frac{\partial\psi}{\partial y}\frac{\partial}{\partial x}\Big)\Big(\frac{1}{h}\frac{\partial\psi}{\partial x}\Big)-k\Big(\frac{\partial\psi}{\partial y}\Big)^2=-h\frac{\partial p}{\partial y}-\frac{\partial h\langle v'^2\rangle}{\partial y}-\frac{\partial\langle u'v'\rangle}{\partial x}+k\langle u'^2\rangle-\frac{1}{Re}\frac{\partial\nabla^2\psi}{\partial x}, \tag{3c}$$

$$\nabla^2=h^{-1}[\partial/\partial x(h^{-1}\partial/\partial x)+\partial/\partial y(h\partial/\partial y)], \tag{3d}$$

with ∇^2 expressing the Laplacian (cf. [6], p. 81). For fully developed turbulent flow as considered here in (3) the gradients of the viscous stresses are asymptotically small compared to the Reynolds stresses outside the viscous wall layer, cf. Subsect. 1.1. It is this region that accounts for the usual no-slip and no-penetration conditions,

$$u=u'=v=v'=0 \quad \text{at} \quad y=0. \tag{4}$$

Furthermore, the external bulk flow is presumed to be strictly irrotational in order to avoid unnecessary difficulties in the subsequent analysis, as becomes clear further below. Moreover, the Reynolds stresses outside the boundary layer are much (i.e. asymptotically) smaller than within. Specifically, we adopt the rather weak assumptions

$$u\sim U_e(x),\ \ u'\sim v'\sim 0 \quad \text{at} \quad y=\delta(x;Re), \tag{5a}$$

and

$$\partial v/\partial x-\partial(hu)/\partial y\sim 0 \quad \text{for} \quad y\geq\delta(x;Re). \tag{5b}$$

Relationship (5b) expresses the requirement of negligibly small vorticity in the external flow.

2 Basic asymptotic analysis and boundary layer structure

As already mentioned in Subsect. 1.1, it is a primary task of the present work to investigate the system of equations given by (3), (4), (5) on condition that the basic Hypothesis 2 holds in the limit (1). To this end, we exploit this conjecture supplemented with the assumption (2) of a thin shear layer by rigorously applying formal asymptotic methods and assign to each flow region for a specific y-regime a characteristic (x-dependent) turbulent velocity scale.

2.1 Velocity defect region

Roughly spoken, the turbulent boundary layer consists of two flow regimes which distinctly differ in their physical meaning, namely the fully turbulent outer flow regime which comprises the vast part of the shear layer and the (extremely thin) viscous subregion adjacent to the wall.

2.1.1 Outer main layer

Specifically, let u_* denote the local reference velocity scale representative for the outermost main region of the boundary layer such that the Reynolds stresses there are considered as quantities of $O(u_*^2)$. Equations (3) and (5a) supplemented with (7) then show that there the gradient of the Reynolds shear stress $-\partial\langle u'v'\rangle/\partial y$ causes a streamwise velocity deficit, given by U_e-u, of $O(u_*^2/\delta)$ which changes its shape in dependence of y. In agreement with Hypothesis 2, that velocity defect is of $O(u_*)$. As a result, $u_*/\delta = O(1)$ in the outer main region of the boundary layer.

For what follows, this situation of a small velocity defect is conveniently described by the order-of-magnitude estimates based on the introduction of a perturbation parameter ε that measures the magnitude of u_* relative to the imposed flow speed U_e:

$$0 < 1-u(x,y)/U_e(x) = O(\varepsilon), \quad \varepsilon = u_*/U_e \ll 1, \tag{6a}$$

$$\left[\langle u'^2\rangle, \langle v'^2\rangle, \langle u'v'\rangle\right] = O(\varepsilon^2), \tag{6b}$$

$$\delta = O(\varepsilon). \tag{6c}$$

Hence, the outer main part of the boundary layer represents a so-called velocity defect layer since it exhibits an asymptotically small streamwise velocity defect triggered by the Reynolds shear stress gradient that generates vorticity. Therefore, this layer appears to be primarily inviscid and irrotational, and the momentum equations as expressed by (3) subject to the boundary conditions (5a) reduce to Bernoulli's law there in leading order,

$$\partial p/\partial y \sim 0, \quad \partial p/\partial x \sim -U_e\,\mathrm{d}U_e/\mathrm{d}x = O(1). \tag{7}$$

Note that the values of the reference quantities $\tilde{U}$ and $\tilde{L}$ introduced above are chosen such that both U_e and $\mathrm{d}U_e/\mathrm{d}x$ and thus the pressure gradient given by (7) are regarded as quantities of $O(1)$. The velocity defect results from the aforementioned balance between the Reynolds stress gradient and the inertia terms with u linearised about $u = U_e$, so that it represents the dominant correction to (7).

2.1.2 Intermediate layer

The classical Hypothesis 1 allows for a direct match of the expansions of the flow quantities in both the outer main and in the viscous wall layer and is associated with a two-tiered boundary layer structure. But that implies in the case of a more general boundary layer description according to Hypothesis 2 the existence of a further so-called intermediate layer, with the physical meaning that there the dynamics of the turbulence-generating viscous near-wall region is "transferred" into the outermost flow regime, characterised by the relationships (6).

Let us exceed the classical boundary layer concept and presume the existence of that intermediate region, equipped with the respective turbulent velocity scale u_τ. Inspection of the streamwise momentum equation (3b) then reveals a predominantly linear dependence of the shear stress on y, where a distinction between two cases must be drawn: (i) the Reynolds shear stress gradient balances the pressure gradient and, in view of (7), is therefore a quantity of $O(1)$. In this layer then having a thickness of $O(u_\tau^2)$ convective terms and the streamwise velocity component u are asymptotically small, and the contributions to the latter that vary with y are of $O(u_\tau)$. The match with the outer main region then implies that these are of $O(1)$ in the overlap domain, according to (6a), and that $\langle u'v'\rangle = O(\varepsilon)$ in the latter flow region, contrasting with (6b). However, this obviously infringes Hypothesis 2. We thus rule out the possibility (i) by adopting (ii) that also the intermediate flow region represents a velocity defect layer with $u \sim U_e$ and is approximately governed by (7). Then the velocity defect is of $o(1)$ but, according to Hypothesis 2, at least of $O(u_\tau)$. In turn, it can be written as

$$0 < 1-u(x,y)/U_e(x) = \varepsilon W(x;\varepsilon) + O(u_\tau), \quad W \sim W_1(x) + \cdots = O(1). \tag{8}$$

Herein, and in remarkable agreement with the empirically motivated boundary layer concept proposed by Clauser [12], the slight deviation εW of the wall slip velocity from its inviscid contribution $U_e(x)$ is imposed by the solution in the outer main layer which, generally, is suggested to satisfy an appropriate matching condition for the Reynolds shear stress rather than the no-slip condition at its base. Here it varies linearly with y, where $(u_*/u_\tau)^2$ measures the ratio of the thicknesses of the outermost and the intermediate layer. Finally, by (6a) and (8) we distinguish between three-tiered boundary layers having $u_*/u_\tau \gg 1$ and a *moderately large* and classical two-layered ones with a *small* velocity deficit in their outermost main region. The latter are obtained exactly for $u_*/u_\tau = O(1)$, viz., $u_* = u_\tau$, indicating a collapse of the outer and the intermediate layer.

It is necessary to study the flow inside the viscous wall region in order to elucidate the correct scalings of the flow in the velocity defect region, hitherto described by the basic estimates (6)–(8). In particular, we seek the dependence of the principal perturbation parameter ε and the intermediate velocity scale u_* in dependence of Re. Therefore, we next rigorously review the analysis of the viscous flow regime and summarise the results which are relevant for the subsequent investigations of the velocity defect region. For a more extensive presentation the reader is referred to the original literature quoted in Subsect. 1.1.

2.2 Viscous wall layer

Let u_ν be the velocity scale typical for the viscous near-wall region. Since we exclude the possibility of a Prandtl-type laminar boundary layer adjacent to the surface (see Subsect. 1.1), the velocity defect in that region must be of $O(1)$, in order to satisfy the no-slip condition (4). Hypothesis 2 then immediately implies that u is a quantity of $O(u_\nu)$ and the viscous shear stress

$$\tau_{xy} = \frac{1}{Re}\left[\frac{\partial u}{\partial y} - \frac{ku}{h} + \frac{1}{h}\frac{\partial v}{\partial x}\right], \tag{9}$$

cf. the right-hand side of (3b), and the turbulent stresses are of the same order of magnitude in this viscous wall region, namely of $O(u_\nu^2)$. According to (4), the local (positive) wall shear stress reads

$$\tau_w = Re^{-1}\,\partial u/\partial y \quad \text{at} \quad y = 0. \tag{10}$$

By using the conventional notation, we then adopt the resulting wall layer scalings by defining

$$\delta_\nu = \frac{1}{u_\nu Re}, \quad y^+ = \frac{y}{\delta_\nu}, \quad u^+ = \frac{u}{u_\nu}, \quad \tau^+ = -\frac{\langle u'v'\rangle}{u_\nu^2}, \quad p^+ = -\frac{U_e\,\mathrm{d}U_e/\mathrm{d}x}{u_\nu^3\,Re}. \tag{11}$$

Here δ_ν measures the wall layer thickness, and y^+, u^+, τ^+ are regarded as quantities of $O(1)$: we expand

$$[u^+,\tau^+] \sim [u_0^+,\tau_0^+](x,y^+) + \cdots. \tag{12}$$

The streamwise momentum equation (3b) integrated once with respect to y^+ is written as

$$\tau_t^+ \sim \frac{\tau_w}{u_\nu^2} + p^+ y^+ + \delta_\nu \int_0^{y^+}\left[\frac{u_0^+(x,\bar{y})}{u_\nu}\frac{\partial[u_\nu u_0^+(x,\bar{y})]}{\partial x} - \frac{\partial u_0^+(x,\bar{y})}{\partial y^+}\int_0^{\bar{y}}\frac{\partial u_0^+(x,\bar{\bar{y}})}{\partial x}\,\mathrm{d}\bar{\bar{y}}\right]\mathrm{d}\bar{y} + O(\delta_\nu), \tag{13a}$$

$$\tau_t^+ = \partial u^+/\partial y^+ + \tau^+, \tag{13b}$$

where τ_t^+ is the total shear stress. Equations (13) state that in the viscous flow regime the convective terms are found to be negligibly small, namely of $O(\delta_\nu)$, compared to the total stress as $Re \to \infty$. In (13a) terms explicitly indicated by $O(\delta_\nu)$ refer to the effects of surface curvature and normal stresses on the wall layer flow (which appear to have no essential impact on the further analysis). We note that the corresponding equation in y-direction (3c) reduces to the balance $\partial p/\partial y^+ \sim -\partial\langle v'^2\rangle/\partial y^+$ of $O(u_\nu^2)$-terms.

The asymptotic structure of the flow implies the existence of an overlap domain conjoining the fully turbulent outer and viscous inner flow regions as $Re \to \infty$. Then the linear rise of τ_t from the wall caused by the rescaled imposed pressure gradient $p^+(x;Re)$ in (13a) is eliminated by a collapse with the higher-order convective terms when y^+ is sufficiently large due the presumed small velocity defect in the fully turbulent flow region. The latter is characterised by (7) and the balance of the Reynolds shear stress gradient with the therefore linearised convective terms. Also, the viscous stress $\partial u_0^+/\partial y^+$ must vanish for $y^+ \to \infty$. The considerations outlined so far indicate that $-\langle u'v'\rangle$ matches the wall shear stress to leading order at the base of the layer residing above the viscous wall region. One then readily infers the important results that $p^+ \to 0$ as $Re \to \infty$ and both u_ν and u_τ can simply be identified with the skin friction velocity:

$$u_\nu = u_\tau = \sqrt{\tau_w}. \tag{14}$$

A different (more straightforward) argument is the following: the alternative $u_\nu^2/\tau_w \ll 1$ singles out $\tau_t^+ \sim p^+ y^+$ with $p^+ = O(1)$ as the then physically feasible leading-order approximation of (13a), giving $u_\nu = O(Re^{-1/3})$ and $\delta_\nu = O(Re^{-2/3})$. However, by matching this scaling is found incompatible with the small-defect structure holding outside the wall region.

As the flow is assumed to be fully developed and not affected by the pressure gradient in leading order, one usually discards (with some reservation) the purely parametric x-dependence in (12). Bearing reference to (13a), this situation is reformulated more precisely in terms of the expansion

$$[u^+,\tau^+,\tau_t^+] \sim [u_0^+,\tau_0^+,\tau_{t0}^+](y^+) + p^+[u_1^+,\tau_1^+,\tau_{t1}^+](y^+) + O(\delta_\nu). \tag{15}$$

Thus, the equilibrium between the total stress and the wall shear stress the momentum balance (13a) reduces to in leading order is slightly perturbed due to pressure forces as

$$\tau_{t0}^+ = 1, \quad \tau_{t1}^+ = y^+. \tag{16}$$

Matching the quantity $y\,\partial u/\partial y$ to leading order eventually yields the logarithmic law of the wall,

$$u_0^+ \sim \kappa^{-1}\ln y^+ + C^+, \;\; \kappa \approx 0.421, \;\; C^+ \approx 5.6, \quad y^+ \to \infty. \tag{17}$$

Herein the well-accepted empirical values of the von Kármán constant κ and the intercept C^+, referring to a perfectly smooth surface, are obtained from the Princeton superpipe experiments performed by McKeon et al. [15]. Their use is reasonable as the indicated universality of the wall functions $u_0^+(y^+)$ and $\tau_0^+(y^+)$ subject to the equilibrium relationships (16) applies to turbulent pipe flow as well. Note that in the non-classical case $u_*/u_\tau \gg 1$ any unbounded term following the logarithmic one in the asymptotic behaviour (17) would induce a small contribution having a magnitude much larger than u_τ to W in the expression (8) for the velocity defect prevalent on top of the wall layer. As will become clear from the analysis in Sect. 3, such a perturbation is associated with the occurrence of an eigensolution of the same magnitude in the outer defect region. However, since the strength ε of the velocity defect is seen to be determined by some appropriate initial conditions further upstream, such eigensolutions and, in turn, unbounded terms of $o(\ln y^+)$ in (17) can be ruled out. The overlap behaviour of the Reynolds shear stress then follows from substitution of (17) into (3b), here expressed by (13) where we note that $\partial u_0^+/\partial x = 0$, as

$$\tau^+ \sim 1 + \Big(p^+ - \frac{2\kappa}{u_\tau Re}\Big)y^+ + \frac{\mathrm{d}U_e/\mathrm{d}x}{U_e\,u_\tau Re}\Big(\frac{1}{\kappa^2}\,y^+\ln^2 y^+ + \cdots\Big) + \cdots, \quad y^+ \to \infty, \;\; Re \to \infty. \tag{18}$$

This relationship is consistent with the analytical results as to the highest asymptotic accuracy possible so far. For the awkward subtleties concerning the matching process which arise from the logarithmic terms in (17) and (18) we refer to the textbook of Van Dyke [13] and the original work by Fraenkel [14].

The present "derivation" of the logarithmic law (17) in terms of a matching condition on the basis of a few assumptions was preceded in the basic study [4], where similar arguments are adopted. However, it was originally proposed by Ludwig Prandtl on dimensional grounds, which are known fairly well. A different albeit closely related well-established dimensional argument exploits the notion of the absence of a definite length scale in the overlap regime: then the ratio of the mixing length, here in non-dimensional form introduced by

$$\ell = \frac{\sqrt{-\langle u'v'\rangle}}{\partial u/\partial y}, \tag{19}$$

and y is approximately a constant, say,

$$\ell/y \sim \kappa. \tag{20}$$

From (18) and (20) immediately follows (17). Various different attempts have been made in literature in the last decades to underpin (17), all essentially exploiting dimensional arguments to one extent or the other, here cf. [6]. As a definitely different and noteworthy approach, Walker [5] accepted (17) as the starting point for further analysis, substantiated by the preliminary but outstanding study by Walker et al. [16] of the time-dependent dynamics in the wall layer (also cf. Butler et al. [17] and Scheichl & Kluwick [18]).

The streamwise velocities match to leading order provided the well-known skin friction law holds,

$$\gamma \sim \kappa/\ln Re, \;\; \mathrm{d}\gamma/\mathrm{d}x = o(\gamma), \quad \text{with} \quad \gamma = u_\tau/U_e. \tag{21}$$

Here more accurate statements require the understanding of the small-defect structure holding on top of the wall layer. However, the relationships (21) determine the skin friction velocity u_τ and, therefore, finally fix the magnitudes of both δ_ν and the pressure gradient parameter p^+,

$$\delta_\nu = O(\ln Re/Re), \quad p^+ = O(\ln^3 Re/Re). \tag{22}$$

As a further result, the viscous stresses appear to be transcendentally small compared to the Reynolds stresses outside the comparatively thin viscous wall layer.

We additionally remark that the vanishing divergence of the fluctuating part of the velocity field subject to the no-slip condition (4) yields the Taylor expansion

$$u_0^+ \sim y^+ - c^+ y^{+4} + \cdots, \;\; \tau_0^+ \sim 4c^+ y^{+3} + \cdots, \;\; c^+ \geq 0, \quad y^+ \to 0_+, \tag{23}$$

cf. Monin & Yaglom [19], pp. 270–272. This completes the wall layer analysis as the full representation of the standard wall functions $u_0^+(y^+)$ and $\tau_0^+(y^+)$ is beyond the scope of the asymptotic analysis of the time-mean flow.

2.3 External potential flow

Finally, we infer from Subsect. 2.1.1 that the small-defect region induces velocity and pressure perturbations of $O(\varepsilon\delta)$ outside the boundary layer where $y = O(1)$. According to (6) and (5b), there

$$[\psi, p] \sim [\psi_0, p_0](x,y) + \varepsilon^2 [\psi_1, p_1](x,y) + \cdots, \quad \left[\langle u'^2\rangle, \langle v'^2\rangle, \langle u'v'\rangle\right] = o(\varepsilon^2). \tag{24}$$

Hence, ψ_1 and p_1 describe the induced potential-flow perturbations. In turn,

$$\nabla^2 \psi_0 = 0, \quad p_0 = -\left[(\partial\psi_0/\partial y)^2 + h^{-2}(\partial\psi_0/\partial x)^2\right]/2, \tag{25a}$$

$$\nabla^2 \psi_1 = 0, \quad p_1 = -(\partial\psi_0/\partial y)(\partial\psi_1/\partial y) - h^{-2}(\partial\psi_0/\partial x)(\partial\psi_1/\partial x) \tag{25b}$$

by (3a), (3d), and Bernoulli's law as obtained by (3b), (3c). The no-penetration condition, see (4), here implies

$$\psi_0(x,0) = 0. \tag{26}$$

We then obtain the near-wall form

$$\frac{\psi_0}{U_e} \sim y - k\frac{y^2}{2} - \left(\frac{1}{U_e}\frac{\mathrm{d}^2 U_e}{\mathrm{d}x^2} - 2k^2\right)\frac{y^3}{6} + O(y^4), \;\; \frac{p_0}{U_e^2} \sim -\frac{1}{2} + ky + \left(\frac{\mathrm{d}^2 \ln U_e}{\mathrm{d}x^2} - 3k^2\right)\frac{y^2}{2} + O(y^3), \;\; y \to 0, \tag{27}$$

of the imposed potential flow, in agreement with (7). Relationships (25b)–(27) are employed in the more detailed analysis of the boundary layer flow in Sect. 3.

2.4 Shortcomings of the classical theory

The classical flow description is readily recovered by identifying ε with γ, which in view of the above analysis completes a fully self-consistent two-tiered description of the boundary layer flow. It effectively relies on the basic assumptions (6a) in the precise form $1 - u(x,y)/U_e(x) = O(\gamma)$. It is most noteworthy that this theory has proven highly successful in describing strictly attached boundary layers, even under the action of rather "strong" (adverse) pressure gradients (with $\mathrm{d}p_0(x,0)/\mathrm{d}x > 0$) as considered here by (7), cf. [5,6] and, in the context of bluff-body separation, Neish & Smith [20].

However, a more subtle and exemplary situation for smooth streamwise pressure distributions is encountered if one considers the special case of quasi-equilibrium flows in the spirit of Kader & Yaglom [21]. Such flows are of high engineering relevance in applications which are very sensitive to separation, as e.g. diffuser flows. As pointed out in [6], they are characterised by an in streamwise direction rather slowly varying (positive) Rotta–Clauser parameter defined as

$$\beta(x;Re) = -\frac{\delta^* U_e \,\mathrm{d}U_e/\mathrm{d}x}{\tau_w}, \quad \text{with} \quad \delta^* = \int_0^\delta \left(1 - \frac{u}{U_e}\right)\mathrm{d}y \tag{28}$$

denoting the displacement thickness (see [12]). An almost constant value of β expresses the equilibrium between the external pressure forces and the wall shear stress acting on an infinitesimally thin streamwise portion of the boundary layer, which thus exhibits vanishing net momentum flux. According to the classical analysis, we have $\delta^* = O(u_\tau^2)$. Therefore, by noticing (10), one finds that this theory is consistent with the assumption that $\beta = O(1)$. Theoretical/semi-empirical investigations, carried out by e.g. Mellor & Gibson [22], Mellor [23], Head [24], Schofield [25], Skote & Henningson [26], in [6], and by Mikhailov [27], however,

indicate the existence of flows where β becomes very large and which are characterised, amongst others, by a loss of uniqueness. Furthermore, it is suggested in these contributions that the classical approach ceases to be valid in the limit $\beta \to \infty$. It is commonly argued there that this failure is due to a considerable reduction of the wall shear stress τ_w and eventually associated with the occurrence of separated flows.

In the authors' opinion, this conclusion appears questionable for two reasons: (A) the small velocity defect-based formulation is not capable of dealing with the rather sudden increase of the velocity defect and, correspondingly, the boundary layer thickness δ on the verge of separation; (B) the limit $\beta \to \infty$ implies $\delta^*/\tau_w \to \infty$ as $Re \to \infty$, which definitely not necessarily requires u_τ to vanish for high but finite values of Re. It is, among other things, the goal of the work presented to show that the obvious shortcomings of the classical approach are resolved by considering a more general velocity defect (6a) holding in its outer main part, which in turn includes the case $\beta \to \infty$ whereas the skin friction remains finite for high but finite values of Re. That is, the flow then remains attached.

We remark in this connection that turbulent boundary layers with a velocity defect larger than allowed for by the classical Reynolds-number asymptotics have been considered already in a number of investigations. To the authors' knowledge, the first attempt to deal with a velocity deficit of $O(1)$ from an asymptotic viewpoint must be attributed to Melnik [28] who adopted a two-parameter expansion method which, however, was based on a specific closure model. A self-consistent generalisation of this three-tiered boundary layer description was put forward by Scheichl [57]; for the recent developments see [11]: as a central ingredient, here the formal independence of the slenderness of the shear layer on Re leads to a four-tiered boundary layer. On the other hand, Sychev & Sychev [29] proposed a three-layer boundary layer structure similar to the one investigated here but with a different scaling. In their theory the intermediate layer represents the actual boundary layer as it exhibits a velocity defect of $O(1)$. Matching the streamwise velocity with the logarithmic behaviour given by (17) then suggests the expansion

$$[u, -\langle u'v\rangle/\gamma_0^2] \sim [U_0, \tau_0](x,Y) + \gamma_0[U_1, \tau_1](x,Y) + \cdots, \quad Y = y/u_\tau^2 = O(1), \;\; \gamma_0 = u_\tau/U_0(x,0) \sim \kappa/\ln Re, \;\; (29)$$

instead of (8). Here the slip velocity $U_0(x,0)$ is of $O(1)$ and determined by the leading-order problem in the intermediate layer. However, since $\partial U_0/\partial Y \neq 0$, matching of the y-gradients of u or, accordingly, of the Reynolds shear stress, note (19) and (20), clearly gives a mismatch. An analogous inconsistency (not yet resolved) is encountered in the two-tiered but large-defect approach by Afzal [30], see also [31]. More recently, George [32] and George & Castillo [33] developed a so-called *Near-Asymptotics* in order to consider two-tiered flat-plate boundary layers having a large velocity defect, i.e. one which essentially does not depend on Re. In turn, the underlying *Asymptotic Invariance Principle* has also been applied to adverse-pressure-gradient (APG) flows by Castillo & George [34]. In contrast, it is the intention of the present study to explore if and how the model-independent classical asymptotic theory of turbulent boundary layers can be refined and extended on the basis of Hypothesis 2 to flows having a "relatively" or moderately large velocity defect. The different layers then surmount the formal difficulties in the matching procedure, e.g. linked with the proposed expansion (29), as they assign different flow properties to those of the Reynolds shear stress. These have to be satisfied by admissible models/are reflected by the asymptotic investigation of existing ones. Therefore, in the approach followed here each layer has a particular physical meaning.

3 Analysis for $\beta \gg 1$: weakly nonlinear effects of inertia

The outline of this section is subsumed as follows: as a starting point, we discuss the intermediate layer in detail by resorting to the analysis presented in Subsect. 2, where its essential characteristics are basically determined by a match with the wall layer flow delineated in Subsect. 2.2. We then demonstrate that

$$\varepsilon/\gamma \to \infty \quad \text{as} \quad Re \to \infty, \qquad (30)$$

for the non-classical case of a moderately large velocity defect of $O(\varepsilon)$ in the outermost part of the boundary layer according to (6a), whereas the Rotta–Clauser parameter β introduced by (28) becomes correspondingly large. It thus enters the analysis of this flow region as it provides a convenient definition of the defect measure ε. The intermediate layer is necessitated by the expansions in both the latter and the viscous wall layer, which are rich enough to allow for a direct match only in the special case of classical small-defect flows. Hence, for the more general non-classical flows the resulting asymptotic analysis of (3b), (3c) is seen to require the inclusion of higher-order terms (compared to the linearisation of the inertia terms known from the classical analysis) in the outer-layer expansion, in order to reveal all the relevant flow attributes by a correct

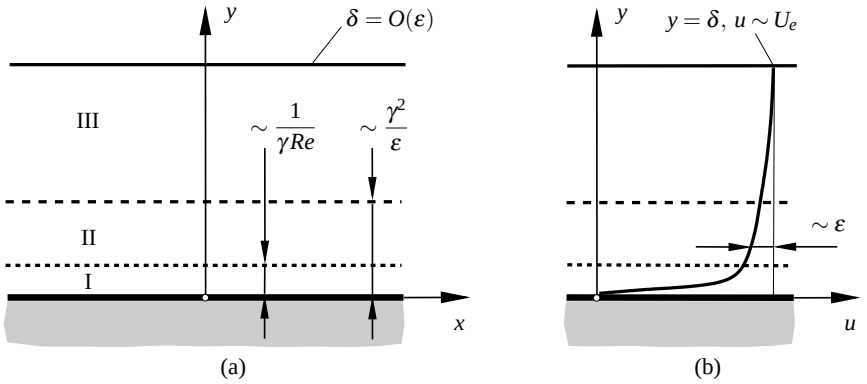

Fig. 2 (a) Asymptotic structure of the boundary layer (viscous wall layer I, intermediate layer II, outer main layer III), having (b) a moderately large velocity deficit of $O(\varepsilon)$

match with the intermediate region. Specifically, this finally allows for the prediction of non-unique boundary layer flows associated with a single pressure distribution.

3.1 Intermediate layer

As in the outermost also in the intermediate flow region the streamwise momentum equation (3b) gives rise to a balance between the Reynolds shear stress gradient and the convective terms, which are linearised about $u = U_e(x)$ and of $O(\varepsilon)$. Inspection of (8), (14) and matching according to (18) then shows that the thickness of the intermediate layer is of $O(u_\tau^2/\varepsilon)$. The thus resulting asymptotic splitting of the boundary layer and the velocity profile are sketched in Figs. 2. Integrating (3b) with respect to the redefined wall-normal coordinate

$$\zeta = \frac{y}{\delta_\tau}, \quad \delta_\tau = \frac{\gamma^2}{\varepsilon}\lambda(x;\varepsilon), \quad \lambda = -\frac{1}{\varepsilon U_e^2}\frac{\mathrm{d}(\varepsilon U_e^2 W)}{\mathrm{d}x} \sim \lambda_1(x) + \cdots, \tag{31a}$$

by taking into account the match with the wall shear stress makes evident that the Reynolds stress varies linearly with increasing wall distance y to leading-order,

$$-\langle u'v'\rangle/u_\tau^2 \sim 1 + \zeta. \tag{31b}$$

Here $\zeta = O(1)$ and $\lambda_1 = O(1)$ in the intermediate layer, in agreement with the expansion of W in (8) and a yet unknown x-dependence of ε. Moreover, the relationship for the velocity defect given in (8) now can be cast into the more precise form

$$1 - u/U_e \sim \varepsilon W(x;\varepsilon,\gamma) + \gamma\hat{u}(x,\zeta). \tag{32}$$

Also, note that contributions to u/U_e of $O(\gamma^2/\varepsilon)$ due to the wall curvature are seen to be of $o(\gamma)$.

Apart from the quantity W, the solution for the intermediate layer is essentially unaffected by the specific flow conditions holding in the main layer, and, in particular, by the distribution of the boundary layer thickness. Dimensional arguments originally put forward by Townsend [35] together with those mentioned in Subsect. 2.2 suggest that ℓ/y then is intrinsically independent of y for $\zeta = O(1)$, i.e. in the region separating the outer main from the viscous wall layer. This is supported also by experimental evidence, see e.g. Skåre & Krogstad [36]. Indeed, matching via the logarithmic portion of the velocity profile given by (17) shows that the well-known original overlap behaviour (20) remains valid across the intermediate layer. Substitution of this linear behaviour for ℓ into (19) and the shear stress distribution (31b) leads in the case $\lambda > 0$, which refers to APG boundary layers and is of interest here, to

$$(\kappa\zeta\,\partial\hat{u}/\partial\zeta)^2 \sim 1 + \zeta. \tag{33}$$

Integration of (33) then yields the generalised law of the wall,

$$\kappa\hat{u} \sim -\ln\zeta + 2\ln\big((1+\zeta)^{1/2}+1\big) - 2(1+\zeta)^{1/2}, \tag{34}$$

where we have for

$$\zeta \to 0: \quad \kappa\hat{u} \sim -\ln(\zeta/4) - 2 + O(\zeta), \tag{35a}$$

$$\zeta \to \infty: \quad \kappa\hat{u} \sim -2\zeta^{1/2} + \zeta^{-1/2} + O(\zeta^{-3/2}). \tag{35b}$$

As far as the behaviour (35b) is concerned, a x-dependent "constant" of integration has been absorbed into the leading-order term εW of the velocity defect represented by (32), so that $\hat{u}$ solely depends on ζ, thus expressing local so-called structural equilibrium (see [35]). In contrast to the classical flow description, here this "slip" term slightly disturbs the "generation gap", see [4], between the expansions of u in the wall layer, see (15), and in the adjoining region. However, it is bridged though by the logarithmic match of $\hat{u}$ according to (17) and (35a).

From (31b) and (32), the y-dependent leading-order contribution to the velocity defect in the intermediate layer is given by $u_\tau\hat{u}(\varepsilon U_e^2\lambda\, y/u_\tau^2)$: by the latter specific form alone the half-power law emerging for $\zeta \to \infty$ is strongly supported on the basis of dimensional considerations as the linear growth of the shear stress with y is presumably tied in with an asymptotic independence of $\hat{u}$ on the skin friction sufficiently far away from the wall. That law was first brought forward by Stratford [37] using closely related arguments, but, in definite contrast, there applied to flows exhibiting vanishing wall shear. As a result, the relation (20) in the limits of, respectively, small and (at least) large values of ζ is backed by the basic Hypothesis 2, with both formal matching and physical intuition (which to a certain degree is subjective by definition, of course) adding as an input.

A universal velocity distribution akin to (34) has been discussed also in earlier attempts to describe the transition of firmly attached towards separated boundary layers, cf. [35,6], Perry et al. [38], and Perry & Schofield [39]. However, the need to introduce an intermediate layer from a thorough asymptotic point of view has apparently not been appreciated so far. This in turn has hampered a consistent extension of the classical theory covering even the case of incipient separation, which is in principle included in the present study.

3.2 Outer main layer

The rather weak variation of γ with x expressed by (21) in combination with (28) suggests the definition $\varepsilon = \gamma\beta_0^{1/2}$, where $\beta_0 = \beta(x_0)$ and $x = x_0$ denotes some selected position at the surface. Here β_0 is taken as known. The half-power behaviour provided by (35b) together with the shear stress distribution (31b) essentially determine the flow in the outermost layer, characterised by a relatively (namely "moderately") large velocity perturbation. Its properties are condensed in (6), and the limit (30) is in hand. Furthermore, it entails that the width of the intermediate layer relative to δ is of $O(1/\beta_0)$, see (31).

3.2.1 Distinguished limit

The shear stress varies predominantly with the distance y from the wall in the overlap with the intermediate layer, and the wall shear stress enters the outer velocity defect solution as a higher-order effect only. Specifically, it becomes a second-order effect if one assumes that $\varepsilon = O(\beta^{-1}) = O(\gamma^{2/3})$, which turns out to characterise the most general case. This is expressed formally in terms of a distinguished (least-degenerate) limit by introducing the coupling parameter

$$\Gamma = \varepsilon\beta_0 = \varepsilon^3/\gamma^2 = O(1), \quad \text{as} \quad \varepsilon = \gamma\beta_0^{1/2}. \tag{36}$$

Then the wall shear stress enters the contributions of $O(\varepsilon^3)$ to the Reynolds shear stress in the outer main layer, as found by matching with the intermediate layer according to (31). The classical case of a small and that of a velocity defect much larger than of $O(\gamma^{2/3})$ are pointed at in the limits $\Gamma \to 0$ and $\Gamma \to \infty$, respectively. We remark that the definitions of β and ε given by (28) and (36) allow for an appealing physical interpretation, cf. [22,11]: expressed dimensionally, the imposed APG determines the "inviscid" reference value $u_p = (\delta^* \mathrm{d}p_0/\mathrm{d}x)^{1/2}$ of the defect velocity, that is, $\beta^{1/2} = u_p/u_\tau$ and $\varepsilon \sim u_p/U_e$.

The effects of both the impressed surface pressure gradient and surface curvature on the boundary layer flow are eliminated advantageously by applying the appropriate small-defect transform in terms of splitting off the contribution of the external bulk flow, viz.,

$$\eta = y/\delta(x;Re), \quad \psi_0 - \psi = \varepsilon\delta U_e F(x,\eta), \quad \left[p_0 - p, \langle u'^2\rangle, \langle v'^2\rangle, \langle u'v'\rangle\right] = -\varepsilon^2 U_e^2 [P,R,S,T](x,\eta). \tag{37}$$

Here η, F, P, R, S, T are taken as quantities of $O(1)$ and ψ_0, p_0 have to be substituted by their Taylor expansions (27) with y being replaced by $\delta\eta$. The nonlinear convective terms in (3) together with (25a) then suggest the (Poincaré) expansions

$$Q \sim Q_1(x,\eta) + \varepsilon Q_2(x,\eta) + \cdots \quad (Q = F, P, R, S, T), \quad \delta/\varepsilon \sim \Delta_1(x) + \varepsilon\Delta_2(x) + \cdots, \tag{38a}$$

$$\beta/\beta_0 \sim B_1(x) + \varepsilon B_2(x) + \cdots, \quad B_1(x_0) = 1, \; B_2(x_0) = B_3(x_0) = \cdots = 0. \tag{38b}$$

For what follows, let σ standing for either 1 or 0 in order to distinguish between the conventional and the extended asymptotic flow description. One has for

$$\sigma = 1: \quad \varepsilon = \gamma \quad \text{(classical small defect)}, \tag{39a}$$

$$\sigma = 0: \quad \varepsilon \gg \gamma \quad \text{(moderately large defect)}. \tag{39b}$$

The definition of ε above refers to case (39b). Most important, case (39a) also draws upon the expansions (38a), but a corresponding generalisation of (38b) amenable to the underlying definition of β_0 requires a subexpansion for

$$\sigma = 1: \quad \beta_0 \sim \beta_{01} + O(\gamma). \tag{40}$$

Inserting (27), (38a), (40) into (37) and the resulting expansions in (3b), (3c), (5) yields by successive integration of (3b) with respect to η a hierarchy of problems: at zeroth order (7) is recovered in exact form when p is identified as p_0, and its i-th member, $i = 1, 2, \ldots$, represents the i-th approximation of (3b). It governs F_1, T_1 for $i = 1$ and F_i, T_i, P_{i-1} for $i > 1$. Also, R_{i-1}, S_{i-1} enter the equations at the i-th level for $i > 1$ only, where they form inhomogeneities. We therefore regard R_i, S_i, T_i as expressed in terms of some functionals which depend on the quantities F_j, $j = 1, \ldots, i$, and their gradients by applying a suitable turbulence model at the i-th level. However, we subsequently adopt an asymptotically correct explicit modelling solely of T_1, for the reason of a numerical representation of the first-order quantities F_1 and T_1.

3.2.2 First-order problem

By noting that $T_1(x,0) = 0$, we obtain the first-order problem

$$\frac{1}{U_e}\frac{\mathrm{d}(U_e\Delta_1)}{\mathrm{d}x}\eta F_1' - \frac{1}{U_e^3}\frac{\partial(U_e^3\Delta_1 F_1)}{\partial x} = T_1 - \sigma, \quad F_1(x,0) = F_1'(x,1) = F_1''(x,1) = T_1(x,1) = 0. \tag{41}$$

Here and in the following primes denote derivatives with respect to η, $\partial/\partial x$ is carried out with η held constant. Problem (41) is characterised by linearised convective terms. The two cases distinguished by (39) result from matching with the flow regions more close to the wall, see Subsects. 2.2 and 3.1. That is, case (39a) applies for ε identified with γ due to the nearly constant total shear stress in the wall layer; also note (15) and (16). An elaborate discussion of this case is given in [4–6], which from here on is considered as far as highlighting the differences in the basic properties of both flow cases is sensible. As a first crucial result, the problem (41) is homogeneous in the case (39b), which is of great significance subsequently.

The boundary conditions for F_1'' and T_1 account for (5b) and (24). As T_1 is expected to be smooth at the boundary layer edge, it has to satisfy the additional requirement $T_1'(x,1) = 0$. However, this does not represent a boundary condition but has to be fulfilled by any asymptotically correct shear stress closure. The mixing-length concept introduced by (19) provides a well-established example for such a closure, which shall be used in the following. That is, $T_1 = (lF_1'')^2$, where the rescaled mixing length $l = \ell/\delta$ to be modelled exhibits a finite limit for $\eta = 1$. Furthermore, problem (41) and hence the quantities F_1, T_1, Δ_1 are unaffected by the surface curvature $k(x)$, at least explicitly. To put this in a more precise way, we note that the magnitude of the velocity fluctuations is of $O(\varepsilon)$ (for the most fractions of time, in accordance with Hypotheses 1 and 2) and their motion is governed by scales much smaller than of $O(1)$. In view of (3), they indeed seem to be uninfluenced by surface curvature to leading order, so that the identical conclusion is drawn for T_1 (and R_1, S_1). Therefore, it effectively seems justified to adopt a commonly employed closure for T_1 that originally has been devised for flows past a planar wall (in contrast to the suggestion made in [6], pp. 602–603, see also Jeken [40]).

In addition, any acceptable closure has to provide the asymptotically correct behaviour $T \sim (\kappa\eta F'')^2$ as $\eta \to 0$ required by (20). Then the match with the wall and the intermediate layer, respectively, implies for

$$\sigma = 1: \quad W_1 - F_1' \sim \frac{\ln\eta}{\kappa}, \quad T_1 \sim 1 + \frac{2\Delta_1}{\kappa U_e}\frac{\mathrm{d}U_e}{\mathrm{d}x}\eta\ln\eta - \left[\frac{\Delta_1}{U_e^2}\frac{\mathrm{d}(U_e^2 W_1)}{\mathrm{d}x} + \frac{\mathrm{d}(U_e^3\Delta_1)/\mathrm{d}x}{\kappa U_e^3}\right]\eta, \quad \eta \to 0, \tag{42a}$$

$$\sigma = 0: \qquad W_1 - F_1' \sim \frac{2}{\kappa}\sqrt{\lambda_1\eta}, \quad T_1 \sim -\frac{\Delta_1}{U_e^2}\frac{\mathrm{d}(U_e^2 W_1)}{\mathrm{d}x}\eta + \frac{2}{3\kappa}\frac{\Delta_1^2}{U_e^3}\frac{\mathrm{d}}{\mathrm{d}x}\Big(\frac{U_e^3}{\Delta_1\lambda_1}\Big)(\lambda_1\eta)^{3/2}, \quad \eta \to 0, \tag{42b}$$

as anticipated by (15) with (17) and (32) in combination with (35b) and (31a), respectively. Hence, the leading-order contribution to the velocity defect $\varepsilon W_1(x)$ in the intermediate layer is part of the solution to the first-order problem (41). Regarding the case (39a), the square-root variation of u with y characterising the overlap of the outer main and the intermediate layer of moderately-large-defect flows is eradicated in favour of the logarithmic one as a consequence of their merging.

Supplemented with an appropriate shear stress closure, a smooth distribution of the inviscid surface speed $U_e(x)$, as well as (non-trivial) initial conditions at $x = x_0$, the resultant well-posed problem (41) for the unknowns Δ_1, F_1, T_1 can be solved numerically by means of downstream integration. In this connection the following observation is important: evaluating (41) at the boundary layer edge $\eta = 1$ and insertion of (38) and (40) into (28) gives the closure-independent relationships

$$(U_e^3\Delta_1 F_{1e})(x) = (\sigma\beta_{01} + 1 - \sigma)C_1 + \sigma\int_{x_0}^{x} U_e^3(s)\,\mathrm{d}s, \quad \text{with} \quad F_{1e} = F_1(x,1), \quad \frac{1}{C_1} = -\Big(\frac{1}{U_e^4}\frac{\mathrm{d}U_e}{\mathrm{d}x}\Big)(x_0). \tag{43}$$

Here the first relation is identified as the leading-order integral momentum equation, where the expression for the positive constant of integration C_1 results from the definition of β_0 given in Subsect. 3.2.1 via (39a) and (36). That is, prescribing $U_e(x)$ imposes a restriction on the possible choices of the initial data for Δ_1 and F_1. Simultaneously,

$$B_1(x) = -\frac{1}{U_e^4}\frac{\mathrm{d}U_e}{\mathrm{d}x}\Big(C_1 + \frac{\sigma}{\beta_{01}}\int_{x_0}^{x} U_e^3(s)\,\mathrm{d}s\Big) \tag{44}$$

governs the variation of β.

In case (39b) the first-order quantities describe a wake-like flow having a moderately large defect as the governing problem (41) is unaffected by the wall shear stress. This quantity is predicted asymptotically for some given value of Re by matching the longitudinal velocity components in the intermediate and the wall layer on the basis of (17) and (32) and the scalings of the flow regions expressed by (11), (14) and (31a), respectively. One then obtains

$$\kappa/\gamma \sim \ln(\gamma\delta_\tau U_e Re) + (\varepsilon/\gamma)\kappa W + \kappa C^+, \quad \mathrm{d}\gamma/\mathrm{d}x \sim -\gamma\varepsilon\,\mathrm{d}W/\mathrm{d}x, \tag{45}$$

and, by inversion, the leading-order form (21) of the sought skin friction law. It is instructive to see how its more precise representations derived from its general form (45) differ in the two flow cases (39): for (39a) its classical form is at play (see e.g. [6]), when δ_τ is formally identified with δ. However, in the case (39b) it is found to be given by the relationship

$$\frac{\kappa}{\gamma} \sim \ln\left(\frac{\gamma^2 U_e^3 Re}{\beta_0^{1/2}}\right) + \beta_0^{1/2}\kappa W_1 + O(\gamma\beta_0), \quad \frac{\mathrm{d}\gamma}{\mathrm{d}x} \sim -\frac{\gamma^2}{\kappa}\frac{\mathrm{d}}{\mathrm{d}x}\big(\beta_0^{1/2}\kappa W_1 + 3\ln U_e\big) + O(\gamma^3, \gamma^4\beta_0). \tag{46}$$

Its classical counterpart is recovered for $\beta = O(1)$, though associated with a singular limit of (46) on account of the aforementioned collapse of the outer layers. In turn, combination of (36) and (46) yields the relationships $\beta_0 \sim (\Gamma\ln Re/\kappa)^{2/3}$ and $\varepsilon \sim \Gamma^{1/3}(\kappa/\ln Re)^{2/3}$. These then enter the expansion of λ, see (31a), as

$$\mathrm{d}\varepsilon/\mathrm{d}x \sim -\varepsilon^2\,\mathrm{d}W_1/\mathrm{d}x \quad \text{and} \quad \lambda_1 = -U_e^{-2}\mathrm{d}(\varepsilon U_e^2 W_1)/\mathrm{d}x, \tag{47}$$

which completes the leading-order analysis.

3.2.3 Second-order problem

Next, we briefly outline the main features of the second-order analysis. It provides the basis for the ultimate subject of the present study, dealt with in the subsequent section. In this context note that due to the vanishing influence of the wall shear stress on the first-order analysis of moderately-large-defect flows its second-order supplement is required to elucidate the basic properties of the flow behaviour. This definitely contrasts with the classical small-defect theory, where such an analysis only yields small corrections of the essential flow picture already captured by the first-order analysis. However, this situation presumably explains why in previous asymptotic investigations of non-interactive turbulent boundary layers with few exceptions (see e.g. [5]) a rigorous treatment of the second-order equations has interestingly not attracted much attention.

At first, we focus on patching the flow quantities at the boundary layer edge, expressed by $\eta = 1$, according to (24), (27) and (37), (38a). This requires the boundary condition $\psi_1(x,0) = -U_e\Delta_1 F_{1e}$ by which the potential-flow disturbance governed by (25b) is induced. From (25) we then infer that $(\partial\psi_1/py)(x,0) = -U_e w$ and $p_1(x,0) = U_e^2 w$ with a non-trivial function $w(x)$ being part of the solution of the induced-flow problem. It describes the negative deviation of the surface slip velocity due to the external flow from its imposed value given by $U_e(x)$. The resultant boundary condition $F_2'(x,1) = w(x)$ then suggests the decomposition

$$F_2 = \bar{F}_2(x,\eta) - w(x)\,\eta, \quad P_1 = \bar{P}_1(x,\eta) - w(x). \tag{48}$$

We note that in higher-order approximations decompositions in line with (48) are introduced advantageously in order to capture the impact of the induced external flow. That is, the defect form (37) proposed originally is gradually compensated for a more nested one when the order is increased.

From (38), (28), and the coupling condition (36) we infer that the rescaled wall shear stress is given by $1/\Gamma = T_2(x,0)$ and that for

$$\sigma = 1: \quad \bar{F}_2'(x,0) = W_2'(x)\,(\not\equiv 0), \quad \sigma = 0: \quad \bar{F}_2' \sim (\Gamma\kappa)^{-1}(\lambda\eta)^{-1/2}, \ \ \eta \to 0, \tag{49}$$

where the latter relationship agrees with (35b). Thus, in the case (39b) the coupling parameter Γ enters the inhomogeneous second-order problem, where the momentum equations (3b) and (3c) assume, after some tedious rearrangements and by virtue of (48), the forms

$$\begin{aligned}
&\frac{1}{U_e}\frac{\mathrm{d}(U_e\Delta_1)}{\mathrm{d}x}\,\eta\bar{F}_2' + \frac{1}{U_e}\frac{\mathrm{d}(U_e\Delta_2)}{\mathrm{d}x}\,\eta F_1' - \frac{1}{U_e^3}\frac{\partial}{\partial x}\big(U_e^3\Delta_1\bar{F}_2 + U_e^3\Delta_2 F_1\big) - T_2 + \frac{1-\sigma}{\Gamma}\\
&= 2\Delta_1 k\eta T_1 + \frac{U_e\Delta_1^2}{2}\frac{\mathrm{d}(k/U_e)}{\mathrm{d}x}\,\eta^2 F_1' - 2\Delta_1^2\frac{\mathrm{d}k}{\mathrm{d}x}\int_0^\eta \bar{\eta}F_1'(x,\bar{\eta})\,\mathrm{d}\bar{\eta}\\
&+ \frac{1}{U_e}\frac{\partial(U_e\Delta_1 F_1)}{\partial x}F_1' - \frac{1}{U_e^2}\frac{\partial}{\partial x}\Big(U_e^2\Delta_1\int_0^\eta\big(F_1'^2 + \bar{P}_1 - R_1\big)(x,\bar{\eta})\,\mathrm{d}\bar{\eta}\Big) + \frac{\mathrm{d}\Delta_1}{\mathrm{d}x}\,\eta(\bar{P}_1 - R_1)\\
&+ \frac{\mathrm{d}W_1}{\mathrm{d}x}\Delta_1(\eta F_1' - 2F_1)
\end{aligned} \tag{50a}$$

and

$$\bar{P}_1 = S_1 + 2k\Delta_1(F_{1e} - F_1), \tag{50b}$$

respectively. Note that Γ is small in the case (39a) but positive throughout. The inhomogeneities at the right-hand side of (50a) are due to the inertia terms in (3b): the second line of (50a) represents the coupling of the first-order defect function F_1 with the surface curvature (where again (41) is employed), in the third line, most important, the nonlinearities come into play, and in the last line the weak variation of ε as predicted by (47). Equation (50b) expresses the balance of the wall-normal gradients of the pressure and the Reynolds normal stress acting in this direction with centrifugal forces. Equations (50a), (50b) are consistent with the boundary conditions

$$\bar{F}_2(x,0) = R_1(x,0) = S_1(x,0) = 0, \quad \bar{F}_2'(x,1) = \bar{F}_2''(x,1) = R_1(x,1) = S_1(x,1) = T_2(x,1) = 0, \tag{50c}$$

by the match with the viscous wall or the intermediate layer, respectively, and patching the flow at the boundary layer edge according to (5a), (5b), (24), and (48). Inspection of (18) and (31b), respectively, confirms the second-order match of the Reynolds shear stress expanded as (38a) and subject to (42) and the resulting behaviour of T_2 for $\eta \to 0$. In addition, we have $\bar{P}_1(x,1) = 0$, which is already satisfied by (50b). Equations (50) then govern the second-order quantities $\bar{F}_2$, Δ_2, and T_2 (when an adequate turbulence closure is applied).

The following should be noted for the sake of completeness: by differentiating (50a) with respect to η we obtain (3b) evaluated at the boundary layer edge in the form $0 = T_2'(x,1) + (\mathrm{d}\Delta_1/\mathrm{d}x)[S_1'(x,1) - R_1'(x,1)]$. As for T_1, we require smoothness also of R_1, S_1, and T_2 in order to enable a smooth transition at the boundary layer edge to the predominantly inviscid external flow. Patching the flow at $\eta = 1$ then suggests the stronger condition $R_1' = S_1' = T_2' = 0$ for $\eta = 1$. This supplement to (50c) has to be accounted for by any suitable turbulence closure, as e.g. the mixing-length-based one introduced in Subsect. 3.2.2.

Eventually, the second-order integral momentum equation is deduced [by evaluation of (50a) at $\eta = 1$ as $\bar{P}_1$ is eliminated with the aid of (50b)]:

$$\begin{aligned}\frac{\mathrm{d}}{\mathrm{d}x}\left(U_e^3\Delta_1\bar{F}_{2e} + U_e^3\Delta_2 F_{1e}\right) &= (1-\sigma)\frac{U_e^3}{\Gamma} + 2\frac{U_e}{k}\frac{\mathrm{d}}{\mathrm{d}x}\left(U_e^2\Delta_1^2k^2\int_0^1 \eta F_1'\,\mathrm{d}\eta\right)\\ &\quad + U_e\frac{\mathrm{d}}{\mathrm{d}x}\left(U_e^2\Delta_1\int_0^1\left(F_1'^2 - R_1 + S_1\right)\mathrm{d}\eta\right)\\ &\quad + 2U_e^3\Delta_1 F_{1e}\frac{\mathrm{d}W_1}{\mathrm{d}x}, \quad \text{with} \quad \bar{F}_{2e} = \bar{F}_2(x,1)\end{aligned} \tag{51a}$$

and subject to the initial condition for $B_2(x)$ in (38b), viz.,

$$\frac{1}{U_e}\frac{\mathrm{d}U_e}{\mathrm{d}x}(\Delta_2 F_{1e} + \Delta_1\bar{F}_{2e}) \to \sigma C_2 \quad \text{as} \quad x - x_0 \to 0_+. \tag{51b}$$

The right-hand side of (51b) is a consequence of (39) and (40), with the constant C_2 being here unspecified. Thus, for turbulent boundary layers having a relatively small velocity deficit the asymptotically correct form of the integral momentum equation, which provides a relationship between the wall shear stress, the pressure forces, and the momentum fluxes due to the velocity deficit, is split into (43) and (51). Here the first set of equation relates F_{1e} to Δ_1, and the second $\bar{F}_{2e}$ to Δ_2 (after integration). We note that the functions $\Delta_1(x)$ and $\Delta_2(x)$ can be regarded as "eigenvalues" of the problems posed by (41) and (50) (and a suitable closure for T_1, T_2), respectively (and are thus parts of their solutions).

In view of obtaining the quantities F_1, Δ_1 and $\bar{F}_2$, Δ_2 by downstream integration, moderately-large-defect flows represent a singular case as neither $F_{1e}(x_0)$ and $\Delta_1(x_0)$ nor $F_{2e}(x_0)$ and $\Delta_2(x_0)$ can be prescribed independently. This finding together with the relationships (51) plays a telling role for what follows.

3.3 Quasi-equilibrium flow and double-valued solutions

Its multi-layered structure inhibits a turbulent boundary layer from assuming a state of full equilibrium of the flow as expressed by self-similar solutions of the leading-order boundary layer equations governing their laminar counterpart. Different states of equilibrium are observed in the wall and the intermediate layer as recognised by the definitions of the suitably rescaled wall layer variables y^+ and ζ, see Subsects. 2.2 and 3.1, respectively. The weak but permanently present variation of γ with x, see (46), reflects the different conditions of equilibrium regarding the leading-order flow quantities describing the wall layer and the relatively small velocity defect outside.

Below our focus is on the outer main layer. The notation "quasi-", "near-" or "pseudo-equilibrium" in the sense of Clauser [41,12], Mellor & Gibson [22] and Kader & Yaglom [21] is commonly used to characterise boundary layer flows having, roughly spoken, $\partial F/\partial x \sim 0$, $\partial T/\partial x \sim 0$ (apparently, the latter authors had this notion in mind when first coining this notion). However, from an asymptotic viewpoint, a more precise definition is preferable: the flow is in strict equilibrium as far as the leading-order solution is concerned if

$$\partial F_1/\partial x \equiv \partial T_1/\partial x \equiv 0, \tag{52a}$$

and in strict equilibrium up to second order if

$$\partial\bar{F}_2/\partial x \equiv \partial T_2/\partial x \equiv 0 \tag{52b}$$

also (when the limit $\varepsilon \to 0$ is described by a single streamwise length scale). Weak dependences of the field quantities on x then are delayed to higher-order effects. A reasonable and precise definition of quasi-equilibrium then emerges quite naturally by requiring (52a), but not necessarily (52b).

3.3.1 First-order problem: external flow, solution, comparison with experiments

The classical theory is recovered for $\beta = O(1)$ and established on the basis of (38), (39a), (40), and (41) subject to (52a). It predicts

$$B_1 \equiv 1, \quad \Delta_1 F_{1e} = (1+3\beta_{01})\,x, \quad U_e = Ex^m \quad \text{with} \quad E = (-C_1 m)^{1/3} x_0^{-m-1/3} > 0, \tag{53a}$$

$$m = -\beta_{01}/(1+3\beta_{01}), \quad \text{with} \quad -1/3 < m < \infty \quad (\infty > \beta_0 > -\infty). \tag{53b}$$

Here the form of the constant E follows from (43), and F_1, T_1 satisfy

$$(1+2\beta_{01})\eta F_1' - F_1 = F_{1e}(T_1 - 1) \tag{54}$$

as (41) reduces to a two-point boundary value problem, cf. [5,6]. The virtual origin $x = \eta = 0$ (chosen without any loss of generality) designates a singular point of the original first- and second-order boundary layer problems (41) and (50), to be regarded (in an asymptotic sense) as the location of laminar–turbulent transition. From this ensues $x_0 > 0$ consistent with the positiveness of E, but the actual value of x_0 remains unspecified in the following. The relationship between m and β_0 in (53b) for the respective surface speed $U_e(x)$ of power-law type in (53a) agrees with (43) and (44), which passes smoothly through the singular case $m \to 0$ of the flat-plate boundary layer. We first consider the external flows, proportional to the free parameter E, that entail such a surface speed $U_e(x)$.

A possible, albeit approximative, realisation of such flows along curved surfaces as shown in Fig. 1 (a) was envisaged by Scheichl & Kluwick [42]. However, then the singular point $x = 0$ apparently has no physical meaning. Contrarily, though technically of less relevance, the class of potential flows along two planes forming a corner as they intersect in the origin ($k \equiv 0$ for $x \neq 0$) are well known to exactly meet the requirement of a power-law flow as in (53a), where we refer to Figs. 1 (b, c). These flows have the representation

$$\psi_0 = E\,\mathrm{Im}(z^{1+m})/(1+m), \quad z = x + \mathrm{i}y, \quad \alpha = \pi m/(1+m). \tag{55}$$

For $m > 0$ / $m < 0$ we deal with boundary layers under favourable/adverse pressure gradients that evolve from the apex of wedges/convex corners. In the first case, see Fig. 1 (b), the real flow picture is regarded as symmetric: otherwise, a rigid surface replacing the line of symmetry ahead of the apex would be physically only consistent with gross separation of the resultant (laminar) boundary layer a distance of $O(1)$ upstream and thus inconsistent with the originally proposed flow picture. Here the only exception conceivable is included in the special case of sufficiently small values of $|m|$, more precisely for a turning angle α of $O(Re^{-1/4})$ (and purely laminar flow), where triple-deck theory applies as considered by e.g. Smith & Merkin [43] and surveyed by Sychev et al. [44], pp. 71–90: then the recirculation bubble has a correspondingly small streamwise extent of $O(Re^{-3/8})$, and reattachment is probably associated with rather rapid laminar–turbulent transition and the formation of a (quasi-)equilibrium turbulent boundary layer further downstream. On the other hand, in the special configuration of a planar wall perpendicular to the line of symmetry for $m = 1$ the aforementioned flow in the vicinity of a stagnation point flow is recovered. For $m > 1$ ($\alpha > \pi/2$) the wedge is interpreted as a corner with the flow impinging on its concave side. However, our major interest concerns the second case, see Fig. 1 (c), where $\mathrm{d}p_0(x,0)/\mathrm{d}x \geq 0$ for $x > 0$. Here the assumption of an oncoming boundary layer ($x < 0$) that already exhibits fairly developed turbulence seems crucial for $-m \gg Re^{-1/4}$ since this is considerably less prone to the undesired massive separation a laminar one undergoes a distance of $O(Re^{-4/9})$ downstream of the apex, see the study of corner flows in [44], chap. 2, and the surprisingly related one by Scheichl et al. [45]. However, a fundamental understanding of a flow around a corner with $\alpha = O(1)$ withstanding separation in the limit (1) is still lacking. Thus, this configuration cannot be put forward confidently as a realistic scenario for the generation of decelerating fully developed turbulent boundary layers satisfying (52a). Finally, in the here interesting extreme case $m = -1/3$ ($\alpha = -\pi/2$) of the strongest APG possible, the potential flow bends over a 90°-knee in clockwise direction.

In summary, corner flows parametrised by the apex angle represent an attractive species of potential flows as they cover the whole domain of m given by (53b) but are in general inhibited by boundary layer separation already upstream of laminar–turbulent transition. Therefore, a more reliable member has been provided by [42], but in that case the surface speed is expected to adjust to the desired power-law form for $x = O(1)$ on a relatively short scale encompassing the virtual origin.

The relationships (53b) imply a breakdown of the classical small-defect approach when the equilibrium parameter β_0 is sufficiently large. As realised first in [22,23], the corresponding limiting behaviour

$$m \sim -1/3 + 1/(9\beta_{01}) + O\big(\beta_{01}^{-2}\big), \quad \beta_{01} \to \infty, \tag{56}$$

suggests expansions of the field quantities in the form of (38) with ε defined as in (36). Unfortunately, however, the two-layer structure adopted in these investigations and also in the more recent corresponding study by Henkes [46] must be considered with scepticism as the defect becomes quite large according to (36) and thus prevents an asymptotically correct treatment of the near-wall regime. These difficulties can be overcome by the present three-layer approach by extending the classical results for equilibrium flows into the large-β regime on the basis of (56), where the flow is parametrised by Γ rather than β_{01}. This affects the second-oder problem (50) in the case (39b), as shown below. Therefore, it is paramount for a comprehensive understanding of this situation to consider self-preserving solutions of (41) in case of (39b). By setting $U_e = \hat{U}(x)$, $F_1 = \hat{F}(\eta)$, $\hat{F}_e = \hat{F}(1)$, $T_1 = \hat{T}(\eta)$, and taking into account (43) and (56), one then obtains

$$B_1 \equiv 1, \quad \Delta_1 \hat{F}_e = 3x, \quad \hat{U} = (C_1/3)^{1/3} x^{-1/3}, \tag{57}$$

$$2\eta \hat{F}' = \hat{F}_e \hat{T}, \quad \hat{F}(0) = \hat{T}(0) = \hat{F}'(1) = \hat{T}(1) = 0. \tag{58}$$

Relations (53) and (57) provide the necessary conditions for strict equilibrium in leading order, expressed by (54) and (58). The case (39b) turns out to be singular in the sense that (57) sorts out the remaining possibility $m = -1/3$ from (53) as (58) just represents the large-β_0 limit of (54). At this stage the specific definition of ε in (39a) and (36), leading to that of $B_1(x_0)$ in (38b), that of C_1 in (43), and finally to (44) and the relations between Δ_1 and F_{1e} in (53a) and (57), proves advantageous: it conveniently implies a unique non-trivial solution of the homogeneous problem (58), having $\hat{F}(1) > 0$, when supplemented with a closure for $\hat{T}$. In turn, the quantities $\hat{U}$, $\hat{F}$, $\hat{F}_e$, $\hat{T}$ represent the canonical first-order solution for moderately-large-defect flows.

To solve problem (58), a local algebraic mixing-length closure is chosen as a most simple representative for the model already indicated in Subsect. 3.2.2. That means that

$$T = l(\eta)^2 F''^2, \quad l = \ell/\delta, \quad \text{with} \quad 0 < l(1) < \infty, \quad \lim_{\eta\to 0}(l/\eta) = \kappa \tag{59}$$

in agreement with (20), here leading to $\hat{T} = l(\eta)^2 \hat{F}''^2$. Then integration of (58) yields

$$\hat{F} = \frac{1}{2\hat{F}_e} \int_0^\eta \left[\int_{\bar{\eta}}^1 \frac{\bar{\bar{\eta}}^{1/2}}{l(\bar{\eta})} \mathrm{d}\bar{\bar{\eta}} \right]^2 \mathrm{d}\bar{\eta}, \quad \hat{F}_e = \left(\frac{1}{2} \int_0^1 \left[\int_\eta^1 \frac{\bar{\eta}^{1/2}}{l(\bar{\eta})} \mathrm{d}\bar{\eta} \right]^2 \mathrm{d}\eta \right)^{1/2}. \tag{60}$$

Specifically, we adopt the well-known model by Michel et al. [47] in the form

$$l(\eta) = c_\ell I_K(\eta)^{1/2} \tanh(\kappa\eta/c_\ell), \quad \text{with} \quad c_\ell = 0.085, \quad I_K(\eta) = 1/(1+5.5\,\eta^6). \tag{61}$$

Herein the well-known intermittency factor $I_K(y/\delta)$ by Klebanoff [48], which accounts for the decrease of the mixing length (and thus for an improved flow prediction) near the boundary layer edge, supplements the original mixing-length distribution proposed in [47] ($I_K \equiv 1$). In fact, calculations employing the classical almost constant mixing length in the outer defect region yield a slightly slower decay of F' near $y = \delta$ and thus appear to overestimate the boundary layer thickness. (This observation not only holds for equilibrium flows.) However, the measurements of near-equilibrium boundary layers at different x-stations, i.e. for different values of β, by Skåre & Krogstad [36] used for comparison in Fig. 3 (a) disclose a rather spontaneous re-increase of l at the very outer part of the defect layer (with some caution as the flow is heavily intermittent). In addition, these authors not only give support for the long-standing broadly adopted estimation $\kappa \approx 0.41$ but also assess the value of l/y to "increase rapidly through the logarithmic layer to a value of" approximately 0.78. This figure is determined by extrapolation of their data of β up to the (still moderate) maximum value achieved of approximately 21.4 to larger values. It was also allotted to κ by Granville [49] in the course of modelling the effect of strong pressure gradients on ℓ. Both variations of l are on the one hand possibly due to the fact that the boundary layer they measured is still not in perfect equilibrium according to (52a), i.e. likewise reminiscent of upstream history, higher-order and free-stream effects. Even more important in the context of an asymptotic theory, their experimental setup allows for values of m not smaller than -0.22 and rather moderate Reynolds numbers based on the momentum thickness below 54000. On the other hand, however, Skåre & Krogstad [36] concur with Perry et al. [38] on the finding that the value of κ in the logarithmic behaviour (17) remains unaffected by external-flow conditions even in the case of a rather strong APG, as of interest here. In addition, they mention that convective effects significantly contribute to the equilibrium attributed to Townsend [35] and detected immediately above the flow region where (17) is observed. Let us mention that these latter statements are excellently confirmed by the asymptotic analysis of Subsects. 2.2 and 3.1. Hence, in view of the quite moderate values of β available in [36] the considerations preceding (33)

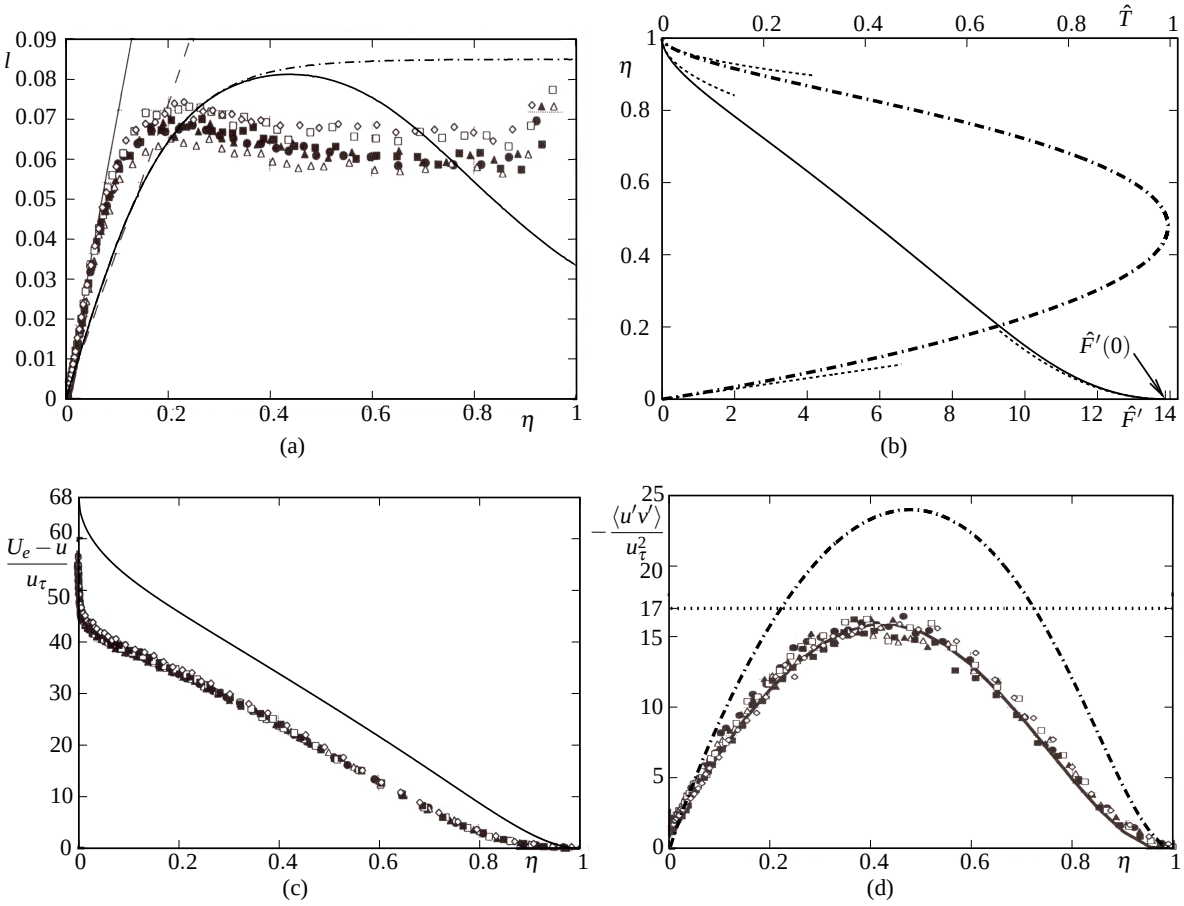

Fig. 3 (a) Mixing length l by (61) (*solid*), from [47] ($I_K \equiv 1$, *dash–dotted*), and from [36] (values of β: ▲19.6, ●19.9, △20.0, □20.1, ■20.2, ◇21.2) with near-wall asymptote (20) for $\kappa = 0.41$ (*dashed*) and "intermediate" fit $l/y \sim 0.78$ (*thin solid*); first-order equilibrium: (b) velocity defect (*solid*) and shear stress (*dash–dotted*) distributions with asymptotes in $\eta = 0$ and $\eta = 1$ (*dashed*), (c, d) data points by [36] (see (a) for caption) with large-β asymptotes (62) (see (b) for caption) for $\beta = 24.1$, (d) calculated shear stress (*solid*) from [36] and close upper bound of measured data (*dotted*)

on the variation of ℓ and its support by the data seem appropriate. Here we have substituted in (61) the value of κ provided by [15] and given in (17).

The resulting closure for ℓ used in the following provides the primary source for quantitative discrepancies between experimental data and our numerical results. Without doubt, however, extending (20) in the form that κ is regarded as a function of ζ having the limiting values of approximately 0.41 and 0.78 as $\zeta \to 0$ and $\zeta \to \infty$, respectively, points to a noteworthy alternative. Moreover, a more complex turbulence model applying to the fully turbulent defect region can be adopted without any principal difficulty. Here we stress that its specific choice has no essential qualitative effect on the asymptotic results as long as (20) is satisfied in the overlap with the viscous wall layer, with ℓ locally *defined* by (19).

Numerical evaluation of (60) yields $W_1(x) = \hat{F}'(0) \doteq 13.868$ for the wake deficit at the wall, $\hat{F}(1) \doteq 5.682$, and $\mathrm{d}\Delta_1/\mathrm{d}x = 3/\hat{F}(1) \doteq 0.528$. In Fig. 3 (b) the resulting self-similar profiles of $\hat{F}'$ and $\hat{T}$ are plotted. The latter clearly signals the onset of a wake-type flow, exerting relatively small skin friction, whereas the distribution of $\hat{F}'$ at first sight is still of typical small-defect type. However, the two inflexion points where $\hat{F}''' = 0$ already bring that wake-like structure to mind. (Still, they are hardly visible, while plotting η over $\hat{F}'$ in landscape style aims at highlighting the details of the curve.) The asymptotes indicate that both $\hat{F}$ and $\hat{T}$ vanish quadratically as $\eta \to 1$ since $\hat{T}(1) = \hat{T}'(1) = 0$ as mentioned in Subsect. 3.2.2, that $\hat{F}'$ exhibits a square-root behaviour as $\eta \to 0$, and the linear rise of $\hat{T}$ as predicted by (42b). The shear stress takes on its maximum value within the fully turbulent flow region rather than at its base, as it is generally the case for classically scaled wall-bounded turbulent flows. Therefore, despite the finite wall shear stress the wake-like velocity distribution qualitatively

resembles separating flow profiles, see Stratford [37,50]. The difference between measured and numerical data in Fig. 3 (a) is also recognised from the comparison shown in Figs. 3 (c, d), based on the classical scaling. For the representation of the leading-order asymptotes,

$$[(U_e-u)/u_\tau,\,-\langle u'v'\rangle/u_\tau^2]\sim[\beta^{1/2}F_1',\,\beta T_1],\quad \beta\to\infty, \tag{62}$$

the maximum value 24.1 of β recorded by Skåre & Krogstad [36] was used. As mentioned before, this seems still inadequately high since the resulting value of the shear stress maximum exceeds its measured counterparts by nearly 50%. On the other hand, the shear stress curve these authors computed via evaluation of the ad-hoc boundary layer approximation of (3) for flat-surface flow,

$$u\,\partial u/\partial x+v\,\partial u/\partial y\sim U_e\,\mathrm{d}U_e/\mathrm{d}x-\partial\langle u'v'\rangle/\partial y, \tag{63}$$

perfectly matches the measurements, as seen from Fig. 3 (d). This supports the reliability of these data and the merit of the experimental efforts by Skåre & Krogstad [36]. Our final conclusion is that any significant difference between the measured data available and the asymptotic results is largely caused by the rather weak rate of convergence towards the latter due to the logarithmic dependence of ε (i.e. the velocity defect) on Re.

We next turn to the second-order perturbations, discussed for general flows in Subsect. 3.2.3.

3.3.2 Second-order problem: solvability condition

In a first step, we consider the constant slope $\Sigma_1=\mathrm{d}\Delta_1/\mathrm{d}x$ in (53a) and (57). It is related to F_{1e} or $\hat F_e$ as for

$$\sigma=1:\quad \beta=O(1),\quad \Sigma_1=(1+3\beta_{01})/F_{1e}, \tag{64a}$$

$$\sigma=0:\quad \Gamma=O(1),\quad \Sigma_1=3/\hat F_e. \tag{64b}$$

The relationships (64a) refer to the classical two-layer theory and hold for $m+1/3=O(1)$. As one infers from (36) and (56), they are replaced by (64b) when the velocity defect becomes so large that $\beta=O(\gamma^{-2/3})$ and the novel three-layer flow description applies. Then Γ supersedes β_0 as the similarity parameter of $O(1)$, whereby the condition of equilibrium affects the second-order analysis. In order to address this situation in an asymptotically accurate and comprehensive manner, we most generally postulate that

$$U_e=(C/3)^{1/3}x^m=\hat U(x)x^\mu\sim\hat U(x)[1+\mu(x)\ln x+\cdots],\quad m=-1/3+\mu,\quad \mu\sim\gamma^{2/3}\mu_1(x)+\cdots=O(\varepsilon). \tag{65}$$

Remarkably, the weak deviation of m from its critical value, $-1/3$, introduces a correspondingly weak but rather exceptional Reynolds-number dependence of the imposed potential flow, described by the at first rather arbitrarily chosen quantity μ_1, which requires a careful revision of the second-order problem (50). A streamwise variation of μ_1 is included in (65) for the sake of generality. Needless to say that also in the case (64a) the second-order analysis can be affected by a weak dependence of m on γ akin to that in (65). However, as turns out below, such a disturbance has a decisive impact on the second-order relations for moderately-large-defect flows only while these are affected only passively in the classical theory.

The relations (64) allow for rewriting the second-order streamwise momentum equation (50a) on condition (52a) in the form

$$\begin{aligned}
&\frac{m+1}{\Sigma_1}\eta\bar F_2'+\frac{x^{-m}}{\Sigma_1^2}\frac{\mathrm{d}(x^m\Delta_2)}{\mathrm{d}x}\eta F_1'-\frac{x^{-3m}}{\Sigma_1}\frac{\partial}{\partial x}\Big(x^{3m+1}\bar F_2+x^{3m}\frac{\Delta_2}{\Sigma_1}F_1\Big)-\frac{T_2}{\Sigma_1^2}\\
&=\frac{1-\sigma}{\Sigma_1}\left[\frac{3x}{\Gamma^{1/3}}\frac{\mathrm{d}}{\mathrm{d}x}\Big(\mu_1(x)\ln x\Big)\hat F-\frac{1}{\Sigma_1\Gamma}\right]\\
&+\frac{2xk}{\Sigma_1}\eta T_1+\frac{x^{m+2}}{2}\frac{\mathrm{d}(x^{-m}k)}{\mathrm{d}x}\eta^2F_1'-\frac{4}{x^{m-1}}\frac{\mathrm{d}(x^{m+1}k)}{\mathrm{d}x}\int_0^\eta\bar\eta\bar F_1'(\bar\eta)\,\mathrm{d}\bar\eta-\frac{2}{x^{2m-1}}\frac{\mathrm{d}(x^{2m+1}k)}{\mathrm{d}x}\eta(F_{1e}-F_1)\\
&+\frac{m+1}{\Sigma_1}F_1F_1'-\frac{2m+1}{\Sigma_1}\int_0^\eta\big(F_1'^2-R_1+S_1\big)(\bar\eta)\,\mathrm{d}\bar\eta+\frac{\eta}{\Sigma_1}(S_1-R_1).
\end{aligned} \tag{66a}$$

This equation is valid for $-1/3\le m<\infty$. Specifically, m stands for the lower bound $-1/3$ in the singular case (64b), in consistency with (65). The correction to $\hat U$ therein adds a contribution to (66a) that stems from the first-order momentum equation in (41), with the coupling between γ and ε introduced according to (36).

In the derivation of (66a) we have eliminated $\bar{P}_1$ with the help of (50b), where we (tentatively) assumed that (52a) implies $\partial R_1/\partial x \equiv \partial S_1/\partial x \equiv 0$.

We are particularly interested in flows which are in equilibrium up to second order. As a necessary condition for maintaining (52b), the inhomogeneous right-hand side of (66a) must be independent of x. Hence, the curvature-dependent contribution has to satisfy the condition

$$k = \hat{K}/x. \tag{66b}$$

Here $\hat{K}$ denotes a free parameter such that values $\hat{K} = 0$, $\hat{K} < 0$, and $\hat{K} > 0$ refer to the cases of a, respectively, plane, concave, and convex surface, cf. Fig. 1 (a). The implications on the external potential flow resulting from the restriction (66b), apart from the corner or "exact" power-law flows addressed above in Subsect. 3.3.1 and by Figs. 1 (b, c), are elucidated in detail in the aforementioned study [42]. There particular emphasis is placed on the limiting case $m = -1/3$, see (57). In the current context one should note that this semi-analytical/numerical study may possibly be of interest in connection with diffuser design and optimisation. Full numerical investigations in this area have been carried out by Lim & Choi [52]: they predicted diffuser shapes which are optimal in the sense that separation is significantly reduced or even avoided for a maximum pressure recovery by both solving the Reynolds equations (3) where they employed a two-point closure and performing a Large-Eddy Simulation. Results of practical relevance reported in the numerous earlier semi-empirical studies of turbulent flows past curved walls as, to note representative experimental ones, by Meroney & Bradshaw [53] and Ramaprian & Shivaprasad [54], corroborate the long-standing interest of engineers in optimised diffuser wall contours.

Regarding the case (64a), a wall curvature (66b) is consistent with (52b) without any further restrictions, as the short-scale adjustment of the flow close to the virtual origin (commented on before) only affects terms of $o(\varepsilon)$ in (38a). This is easily seen from (66) and more concisely from the second-order integral momentum equation, see (51a). In the present context we conveniently introduce the function $\rho(\eta; m, \hat{K})$ in order to subsume the last two lines of (66a) in the quantity $-\rho/\Sigma_1$ and abbreviate the right-hand side of the momentum equation in (51a) by

$$r(m,\hat{K}) = \Sigma_1 \rho(1; m, \hat{K}) = (2m+1)\Sigma_1 \int_0^1 \left(F_1'^2 - R_1 + S_1\right) \mathrm{d}\eta + 4m\Sigma_1^2 \hat{K} \int_0^1 \eta F_1' \, \mathrm{d}\eta. \tag{67a}$$

Then (51a) becomes

$$x^{-3m} \frac{\mathrm{d}}{\mathrm{d}x}\left(x^{3m+1}\Sigma_1 \bar{F}_{2e} + x^{3m}\Delta_2 F_{1e} + 9\frac{1-\sigma}{\Gamma^{1/3}}\mu_1(x)\ln x\right) = \frac{1-\sigma}{\Gamma} + r, \tag{67b}$$

where in the additional contribution proportional to μ_1, present in (66a) in the case (64b), we have expressed $\hat{F}_e$ by $3/\Sigma_1$. Turning back to (64a), a term arising by integration of (67b) is discarded as then the second contribution to (66a) would vary proportional to x^{-3m-1}, whereas all other terms are constant. We then arrive at the conclusion that (52b) enforces

$$\Delta_2 = \Sigma_2 x, \quad \text{with} \quad \Sigma_2 = const \tag{68}$$

and, in view of (51b), $C_2/x_0 = r/(3m+1)$. Finally, (67b) reads

$$\bar{F}_{2e}/F_{1e} + \Sigma_2/\Sigma_1 = r, \tag{69}$$

where we have used (53) and (64a). Equation (69) represents the second-order counterpart to (53a) as it provides the desired relationship between Σ_2 and F_{2e}. Also, it is readily seen that the classical second-order results are formally unaffected by the quantity Γ.

A different, even more restricted and rather intricate singular situation arises for moderately-large-defect flows captured by (58), (64b), and the limiting case $m = -1/3$ in (66a) and (67). This comes into operation under the assumption (65). As a consequence, by integration of (67b) one obtains

$$3\bar{F}_{2e}/\hat{F}_e + \Delta_2 \hat{F}_e/x = \left(\Gamma^{-1} + \hat{r} - 9\Gamma^{-1/3}\mu_1\right)\ln x + const, \quad \text{with} \quad \hat{r} = r(-\tfrac{1}{3}, \hat{K}). \tag{70}$$

The relationships (70) can be satisfied for any prescribed function $\mu_1(x)$ and values of Re and β_0. These in turn fix the values of γ by (21) and finally Γ as $\Gamma = \gamma\beta_0^{3/2}$ by virtue of (36), while the quantities $\bar{F}_2$, T_2, Δ_2 evolve in streamwise direction in general. For $\Gamma \to 0$ the asymptote $\mu_1 \sim \Gamma^{-2/3}/9$ resulting from (70)

provides the missing match of the external-flow exponent m governed by (65) with (53b) according to (56), i.e. of moderately-large-defect flows close to equilibrium with small-defect flows exhibiting equilibrium to first order. This demonstrates that under the assumption (65) the second-order solutions comprise the continuation of the family of self-preserving flows parametrised by m and originally represented by (53). Therefore, on condition $\mu_1 = const$ we advocate to adopt the notion quasi-equilibrium in the more strict sense that it is even allied with (52b). Conversely, under this premise one infers from (70) that all terms except the second in (66a) are definitely independent of x, as in the classical case (64a). Hence, (68) must hold also for moderately-large-defect flows in order to satisfy (66a). We then have for

$$\sigma = 1: \quad \Sigma_2 = \left(r/F_{1e} - \bar{F}_{2e}/F_{1e}^2\right)/(1+3m), \tag{71a}$$

$$\sigma = 0: \quad \Sigma_2 = -3\bar{F}_{2e}/\hat{F}_e^2. \tag{71b}$$

These relationships between $\bar{F}_{2e}$ and Σ_2 form the complement to (64). Specifically, (71a) results from (69), and (71b) from (70) with (51b), which predicts a vanishing constant under the premises (57) and (68). Simultaneously, the constant of integration in (70) is seen to vanish. Then (70) subject to (65) and (67a) is restated as

$$9\Gamma^{2/3}\mu_1 = 1 + \hat{r}\Gamma, \quad \text{with} \quad \hat{r} = \hat{F}_e^{-1}\int_0^1 (\hat{F}'^2 - \hat{R} + \hat{S})\,\mathrm{d}\eta - 12\hat{K}\hat{F}_e^{-2}\int_0^1 \eta\hat{F}'\,\mathrm{d}\eta. \tag{72}$$

Here Σ_1 is substituted by $\hat{F}_e$ through (65) and $\hat{R} = R_1(\eta)$, $\hat{S} = S_1(\eta)$ denote the normal stresses, as determined on basis of the canonical solution of (58) and contributing significantly to the second-order solution. We then face a constraint between the effective values of the similarity parameter Γ and of μ_1 (for a given surface geometry represented by $\hat{K}$). However, this does not signal a breakdown of the present approach. It rather expresses the physical result that external streamwise velocity distributions of the form given in (57) generate solutions for the streamwise velocity defect which are self-similar in leading order as required and evident by (58), whereas higher-order correction terms are not as these exhibit an explicit x-dependence. In order to achieve self-similarity even up to second order the distribution $U_e = \hat{U}(x)$, therefore, has to be modified, i.e. slightly perturbed according to (65) with μ_1 being constant.

The relationships (72) are interpreted as a solvability condition of (66) as they provide an asymptotically correct criterion for selecting the value of the rescaled first-order velocity defect given by $\Gamma^{1/3} = \varepsilon/\gamma^{2/3}$ in dependence of μ_1. A single parameter $\hat{r}$ of $O(1)$ accounts for nonlinear and curvature effects and has to be calculated employing a complete Reynolds stress closure. However, as indicated by semi-theoretical considerations regarding the budget of the Reynolds normal stresses at the outer edge of the viscous wall layer, see [6], p. 526, the quantity $\hat{S} - \hat{R}$ is expected to be positive for $0 \le \eta \le 1$. Experimental support for this prediction is provided in [36] and by Elsberry et al. [55], who studied turbulent boundary layers exposed to an APG. Their measurements in the fully turbulent defect region which is in equilibrium clearly show that $(0 <) S/R < 1$ for $0 \le \eta \le 1$. Furthermore, a coincident observation is made in the much earlier study [47] on basis of well-known von Kármán's form of the integral momentum equation. As a result, $\hat{r}$ is found to be positive when the value of $\hat{K}$ is smaller than a positive critical value. In the present study we stipulate that $\hat{r} > 0$, which includes the important case $\hat{K} = 0$ of a planar wall. We advantageously introduce the abbreviations

$$\hat{G} = \hat{F}_e^{-1}\int_0^1 \hat{F}'^2\,\mathrm{d}\eta, \quad \hat{H} = 12\hat{F}_e^{-2}\int_0^1 \eta\hat{F}'\,\mathrm{d}\eta, \tag{73}$$

where $\hat{G}$ is the accordingly rescaled equilibrium shape factor, defined in [6], in leading order. It is added that the simple mixing-length closure 61 gives $\hat{G} \doteq 8.053$ and $\hat{H} \doteq 0.663$.

It is illuminating to cast the equilibrium condition given by (72) into the generic form

$$9\hat{D}^2\hat{\mu} = 1 + \hat{D}^3, \quad \text{with} \quad \hat{D} = \hat{r}^{1/3}\Gamma^{1/3}, \ \hat{\mu} = \hat{r}^{-2/3}\mu. \tag{74}$$

Relation (74) is displayed in Fig. 4 (a): most interestingly, the nonlinearities restrict the deviation μ of the power-law exponent m from $-1/3$ to positive values as expressed by the existence of a turning point where $\hat{\mu} = \hat{\mu}^* = 2^{1/3}/6$ and $\hat{D} = \hat{D}^* = 2^{1/3}$. In turn, the double-valued rescaled velocity defect measure $\hat{D}$ reveals a non-unique flow structure, corresponding to a single value of the external-flow exponent m, where the upper and the lower branch point to, respectively, a relatively large and relatively small defect. Also, a non-equilibrium flow connecting two equilibria is indicated qualitatively (and refers to (70) for a non-constant μ_1), and the asymptotes $\hat{D} \sim (9\hat{\mu})^{-1/2}$ and $\hat{D} \sim 9\hat{\mu}$ of the upper and the lower branch, respectively, in the limit

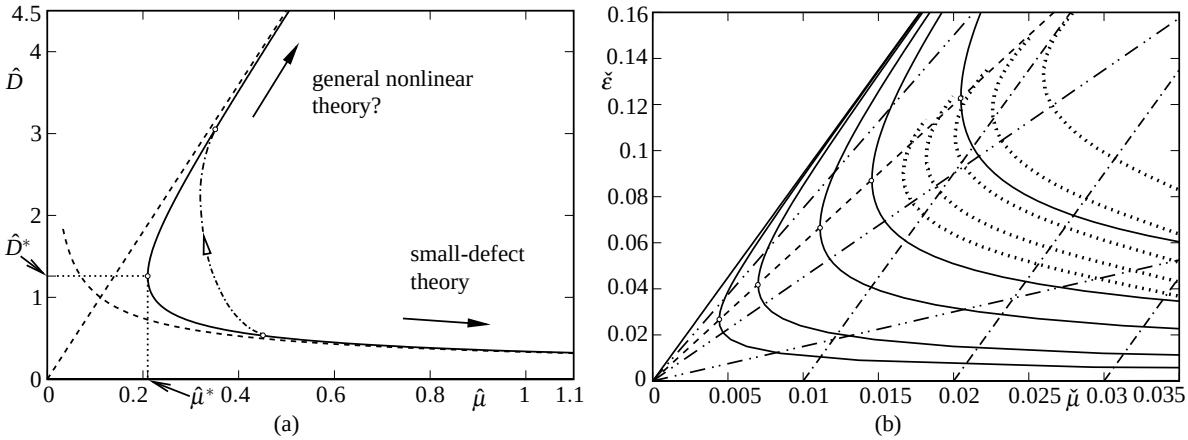

Fig. 4 (a) Canonical relationship (74) including asymptotes (*dashed*) and suggested connection (*dash–dotted*), (b) map of non-unique flow field from (75) with (21), curves from right to left parametrised by increasing numbers: $\lg Re = 6, 10, 15, 30, 60, \infty$ (*solid*) with vertexes connected (*dashed*), $\lg Re = 6, 7, 8, 9, 10$ (*dotted*), $\check{\beta}^{-1} = 0.09, 0.18, 0.27$ (*dash–dotted*), $\check{D}^{-3} = 0.2, 1, 5$ (*dot–dash–dotted*)

$\hat{\mu} \to \infty$ are plotted. As expected from (56), the first provides the aforementioned match with the classical small-defect theory for vanishing nonlinear effects. In contrast, the latter accounts for the increasing influence of nonlinearly coupled inertia terms. This strongly suggests the possibility to formulate a general rational theory of turbulent boundary layers which holds even for a streamwise velocity defect of $O(1)$ and, in turn, includes separating flows. Highly notable in this context, the numerical study accompanying the asymptotic investigation of (self-preserving) turbulent boundary layers on the brink of separation which have a large velocity deficit by Durbin & Belcher [56] predicts a distinctly double-valued wall shear stress for one (rather moderate) prescribed value of β_0.

Also, it is instructive to extract from (72) or (74) via (36) asymptotic relationships that involve the original perturbation parameters ε, μ, and β_0 in normalised form,

$$9\check{\mu} \sim (\gamma/\check{\varepsilon})^2 + \check{\varepsilon} \sim \check{\beta}^{-1} + \check{\varepsilon} \sim \big(1 + \check{D}^{-3}\big)\check{\varepsilon}, \quad \text{with} \quad \big[\check{\varepsilon}, \check{\mu}, \check{\beta}, \check{D}\big] = \big[r^{1/3}\varepsilon, r^{-2/3}\mu, r^{2/3}\beta_0, r^{1/3}\Gamma^{1/3}\big]. \tag{75a}$$

The first of these relates the magnitude of the defect ε to μ in the limit given by (21) and (1). Here the minima $\check{\mu}^*$ of $\check{\mu}$ satisfy

$$6\check{\mu}^* \sim \check{\varepsilon} \sim 2^{1/3}\gamma^{2/3}. \tag{75b}$$

The flow chart in Fig. 4 (b) illustrates the interdependence of the various perturbation and coupling parameters involved in the $(\check{\mu}, \check{\varepsilon})$-space, with asymptotic accuracy of second order and for the numerical value of κ in (17): admissible points lie in the region $\check{\varepsilon} > 0$ bounded by the large-$\check{\mu}$ asymptotes, $\check{\varepsilon} \sim 9\check{\mu}$ and $\check{\varepsilon} = 0$, which here are also viewed as the limiting form of (75a) when (formally) $1/Re = 0$. This inevitably points to the existence of a second "non-trivial" boundary layer limit, mentioned above in connection with a velocity deficit of $O(1)$, aside from the "trivial" potential-flow limit, which is just slightly perturbed by the classical *Re*-dependent small-defect flow structure. In the first case the momentum equations (3) indeed (formally) reduce to (63) in leading order when the empirical slenderness of the shear layer flow provides a small perturbation parameter. However, because the velocity scale representative for the Reynolds stresses is considered as small but independent of *Re*, here the suggestion of an $O(1)$-deficit is received with some reservation as it obviously requires a careful adaption of Hypotheses 2 [hence the interrogation mark in Fig. 4 (a)].

The resulting generalised asymptotic flow description including large velocity defects is a topic of intense current research activities. Its key properties, however, were already highlighted in [57] and restated more precisely in [11] by taking up ideas proposed by Melnik in his study [28] on turbulent separation: cf. the corresponding comments in Subsect. 2.4. As one interesting finding, the upper branch of the $\hat{D}$-versus-$\hat{\mu}$ curve, see (74), is seen to match the corresponding representation of von Kármán's form of the integral momentum equation when applied to self-preserving large-defect (APG) flows, i.e. for $-1/3 < m\,(< 0)$. In the form discussed in [6], this integral relationship is a direct consequence of Melnik's flow structure. Although without being embedded in a strict asymptotic framework, the existence of two-valued self-similar flows then

emerges quite naturally: for a given high but finite value of *Re* its large-defect branch is connected smoothly with the classical small-defect branch via a turning point, here mapped onto $(\hat{\mu}^*, \hat{D}^*)$. We derive and exploit this relationship in Sect. 4.

3.3.3 Second-order problem: solution

The above investigation of flows satisfying strict equilibrium can be summarised as follows: necessary conditions for (52) are represented by (68) and, in particular, by (53) for $\sigma = 1$ and (57), (65) with $\mu_1 = const$, and (72) for $\sigma = 0$. Let (66) be rewritten as

$$\big[(m+1)\eta\,\mathrm{d}/\mathrm{d}\eta - 3m - 1\big]\big(\Sigma_1\bar{F}_2 + \Sigma_2 F_1\big) - T_2 = (1-\sigma)\big(3\Gamma^{-1/3}\mu_1\Sigma_1\hat{F} - \Gamma^{-1}\big) - \Sigma_1\rho(\eta;m,\hat{K}), \tag{76a}$$

with m being $-1/3$ in the singular case $\sigma = 0$ and the eigenvalue Σ_1 of the first-order approximation given by (64). Evaluation of (76a) for $\eta = 1$ recovers the relationships (71) for the eigenvalue Σ_2 and (69)–(72) in combined form as $(3m+1)(\Sigma_1\bar{F}_{2e} + \Sigma_2 F_{1e}) + (1-\sigma)(9\Gamma^{-1/3}\mu_1 - \Gamma^{-1}) = r$, with r introduced by (67a).Then (76a) is subject to the remaining true boundary conditions

$$\bar{F}_2(0) = \bar{F}_2'(1) = 0, \tag{76b}$$

where we add for the sake of completeness that $\rho'(1;m,\hat{K}) = 0$, in agreement with the note on smoothness of the second-order results at $\eta = 1$ subsequent to (50c). The so obtained inhomogeneous two-point boundary value problem has to be closed consistently with the first-order results, i.e. T_2 to be expressed by the accordingly expanded underlying model for T. Here this is conveniently accomplished in the form (59) subject to (38a), which yields the first- and second-order closures $T_1 = l(\eta)^2 F_1''^2$ and

$$T_2 = 2l(\eta)^2 F_1'' \bar{F}_2'', \tag{76c}$$

respectively.

Specific interest is drawn to the moderately-large-defect case $\sigma = 0$. The parametric dependence of the second-order corrections $\bar{F}_2$ and T_2 on β_{01} for (64a) along with (53b) is replaced by that on Γ when (64b) applies. It is seen from (66) that the second-order corrections $\bar{F}_2$ and T_2 then depend on both Γ and $\hat{K}$, unlike the canonical first-order quantities $\hat{F}$ and $\hat{T}$. Conforming to to the notation adopted in (58) and (70), we in turn set $\bar{F}_2 = \hat{\bar{F}}(\eta;\Gamma,\hat{K})$ and

$$\rho(\eta;{-\tfrac{1}{3}},\hat{K}) = \hat{\rho}(\eta;\hat{K}) = -\frac{\hat{K}}{\Sigma_1}\Big(\eta^2\hat{F}' + \frac{4}{3}\int_0^\eta \big[\hat{F}_e - \hat{F}(\bar{\eta})\big]\,\mathrm{d}\bar{\eta}\Big) - \frac{2}{3}\hat{F}\hat{F}' + \frac{1}{3}\int_0^\eta \hat{F}'(\bar{\eta})^2\mathrm{d}\bar{\eta} + \mathrm{RNS}. \tag{77a}$$

Herein RNS abbreviates the contributions of the Reynolds normal stresses and $\hat{T}$ has been eliminated by the use of (58) and (64b). Due to the vanishing coefficient of $\bar{F}_2$ in (76a), the solution of (76) then can be expressed in closed form. We conveniently introduce

$$\hat{J}(\eta;\Gamma,\hat{K}) = \int_0^\eta \hat{F}'(\bar{\eta})^{1/2}\int_1^{\bar{\eta}} \frac{\Sigma_1\big[\hat{\rho}(\bar{\bar{\eta}};\hat{K}) - \hat{\rho}(1;\hat{K})\hat{F}(\bar{\bar{\eta}})/\hat{F}_e\big] + \Gamma^{-1}\big[1-\hat{F}(\bar{\bar{\eta}})/\hat{F}_e\big]}{2(l^2\hat{F}''\hat{F}'^{1/2})(\bar{\bar{\eta}})}\,\mathrm{d}\bar{\bar{\eta}}\,\mathrm{d}\bar{\eta} \tag{77b}$$

in order to obtain by elimination of μ_1 in (76a) through (72) and some manipulations

$$\hat{\bar{F}} = \hat{J}(\eta;\Gamma,\hat{K}) - \hat{J}(1;\Gamma,\hat{K})\hat{F}(\eta)/(2\hat{F}_e). \tag{77c}$$

Here we have again used (58), (64b), and (71b). The relationships (77) together with (71b) represent the second-order complement to the first-order results (60) and (64b). In the special case $\hat{K} = 0$ of flat-plate flow and under the neglect of Reynolds normal stresses, analytical/numerical evaluation of (77b), (77c) indicates that $\hat{\bar{F}}'$ can take on negative values, which remarkably agrees with the deviation of the first-order quantities from the measured data taken from [36], noticed in Figs. 3 (c, d). Also, (77b) manifests the expected collapse of the expansions (38a) when $\Gamma = O(\varepsilon)$, which captures the small-defect case through (36). Contrarily, the expression for $\hat{J}$ shows that in the large-defect limit $\Gamma \to \infty$ the second-order solution remains bounded, so that the finite correction $\hat{\bar{F}}'(0;\infty,\hat{K})$ to the wall slip supersedes the reciprocal half-power behaviour as given in (49). A more detailed study of (77) is under way.

We revisit the second-order analysis in the "Appendix", by pointing out two additional issues for the sake of deepened insight.

4 Comparison with numerical data for finite values of *Re* and measurements

In order to support the asymptotic results predicting multi-valued solutions, a numerical study was performed by solving the boundary layer equations including nonlinear convective terms and assuming strict equilibrium in the fully turbulent flow regime. To this end, we consider APG flows having self-similar form,

$$\eta = y/\delta(x;m,Re), \quad \psi = U_e(x;m)\, f(\eta;m,Re), \quad -\langle u'v'\rangle = U_e^2(x;m)\, t(\eta;m,Re). \tag{78}$$

Here the parametric dependences of the flow quantities are written out once for the sake of comprehension but omitted further below. In the case of zero surface curvature the boundary layer equation (63) exhibiting full inertia terms gives rise to the two-point boundary value problem

$$m(f'^2-1)-(1+m)\,ff''=t'/a, \quad 0<a=\mathrm{d}\delta/\mathrm{d}x=const, \tag{79a}$$

$$\eta\to 0: \;\; f'\sim(\gamma/\kappa)\ln(a\gamma Re\,\eta),\;\; t\sim\gamma^2,\;\; f\sim\eta f', \quad \eta=1: \;\; f'=1,\;\; t=0, \tag{79b}$$

where the external potential-flow velocity $U_e(x)$ satisfies the power law as given by (53a), see e.g. [6]. The boundary conditions for $\eta\to 0$ reflect the logarithmic behaviour, represented by (17) and (21), of the streamwise velocity in the overlap regime between the outer region and the viscous wall layer.

To solve problem (79), it is supplemented with the (asymptotically correct) algebraic mixing-length closure $t=l(\eta)^2 f''^2$ where $l(\eta)$ is again given by (61). Furthermore, we prescribe a (sufficiently large) value of *Re*, a properly chosen (sufficiently small) value of the growth rate a of the boundary layer thickness δ, as well as a minimum value of η which determines the inner boundary of the computational domain, while both γ and the exponent m are regarded as eigenvalues and are thus part of the solution. This procedure allows to compute the expected double-valued solutions for a given pressure gradient characterised by a single value of m. A converged solution successfully serves as the initial guess for a neighbouring one pertaining to a relatively mild increase of a. This finally results in an array of solutions, indexed by consecutive values of a in an appropriate range. We stress that from a strict asymptotic point of view (79a) indeed results from an ad-hoc simplification of the underlying full set of Reynolds equations (3), but nonetheless is anticipated to capture the essential phenomena of the specific equilibrium boundary layer flow under focus for large but finite Reynolds numbers *Re*. These parametrise the solutions solely via the logarithmic near-wall portion of the flow. As a consequence, the asymptotic error is inherently of $O(\gamma)$, where γ has the asymptotic representation (21). Therefore, extending the domain of the calculations to the boundary $\eta=0$ by adopting a wall layer model (to close τ^+) would not improve significantly the quality of the numerical solution when *Re* becomes quite large. Newton iterations applied to an adaptive finite-differences discretisation (advanced deferred-correction technique) of (79) converge to highly accurate solutions: absolute errors of about 10^{-9} at less than 500 grid points for $\eta\in]0,1]$.

By integration of (79) from $\eta=0$ to $\eta=1$, one recovers von Kármán's integral momentum equation, specified for equilibrium boundary layers, in the form

$$\varepsilon G(1+2m)-1-3m=m/\beta. \tag{80}$$

Herein the Rotta–Clauser parameter β introduced by (28) and the equilibrium shape factor G read

$$\beta = am[f(1)-1]/\gamma^2, \tag{81}$$

$$\varepsilon G=\int_0^1 (1-f')^2\,\mathrm{d}\eta\,/\,[1-f(1)]=\varepsilon\int_0^1 F'^2\,\mathrm{d}\eta\,/F(1). \tag{82}$$

The latter relation in (82) is obtained by setting

$$f(\eta)=1-\varepsilon F(\eta), \tag{83}$$

in agreement with (78) and (37). Thus, for a velocity defect of $O(\varepsilon)$ the shape factor G represents a generalisation of its original definition given in [6] in connection with classical small-defect flows, i.e. when ε is replaced by γ. Accordingly, the stretched quantity εG serves as a convenient measure for the strength of the nonlinearities due to convection. We now specify the defect parameter ε in the form

$$\varepsilon=\gamma\beta^{1/2}, \tag{84}$$

which in the limit $\varepsilon \to 0$ under consideration reduces to the earlier definition included in (36) by taking into account the expansion (38b) together with the requirement for B_1 in (57). One then easily verifies that (80) can be rewritten as

$$(1+2m)D^3 = (1+3m)\beta + m, \quad \text{with} \quad D^3 = \gamma\beta^{3/2}G. \tag{85}$$

We note that $D \sim \hat{D}$ and $G \sim \hat{G} = \hat{D}^3/\Gamma$ as $\varepsilon \to 0$, where the defect measure D, its canonical representation $\hat{D}$, and $\hat{G}$ are defined by (85), (74), and (73), respectively. In the limit $m+1/3 \to 0_+$ formulated in (65) the integral momentum equation (85) can then be viewed as a restatement of the asymptotically correct solvability condition given by, respectively, (72) and (74), as the neglect of surface curvature and Reynolds normal stresses yields $r \sim G$.

We see that for given values of Re and m the key parameters β, ε, γ, G, and r are computed from the solution of (79). Non-uniqueness is an immediate consequence of the rightmost terms in (80) and (85), which are due to the rescaled wall shear stress γ^2 and thus reflect the effect of finite values of Re. Let us discuss this situation with the help of (80) by taking β as a function of G for a given value of γ: the assumption of very small values of G, i.e. $\varepsilon G = o(\varepsilon)$, gives rise to the branch referring to the classical small-defect theory, characterised by $\beta = O(1)$: here (53b) is confirmed. If G is increased to $O(1)$ or, equivalently, $m+1/3$ is reduced to $O(\varepsilon)$, we have $G = O(1)$ and arrive at the situation of a moderately large defect: see (75a) and Fig. 4 (b). Finally, $\varepsilon G = O(1)$ implies $\beta \gg 1$ and a velocity defect of $O(1)$. This second branch of the relationship between G and m is dominated by the limiting "inviscid" form of (80), formally obtained in the limit $\beta \to \infty$ and supposed to describe large-defect flows in [6] as outlined at the end of Subsect. 3.3.2. Viewed from this scale, a degenerate small-defect branch emerges for $\varepsilon G \ll 1$ and $-1/3 < m$ due to very small viscous effects.

The plots for $\hat{D}$ versus $\hat{\mu}$ for various Reynolds numbers Re in Fig. 5 (a) were obtained by evaluation of (85), where the Rotta–Causer parameter β was determined in the form (81) from the associated solutions of the boundary layer problem (79). That is, for a prescribed value of Re any dupel $(\hat{\mu}, \hat{D})$ belongs to a single value of the presumed constant growth rate $a = \delta/x$ of the boundary layer (with $x = 0$ again being the virtual origin). The expansion of δ following (38a), where Δ_1 is given by (53a), in combination with (84) and (85) indicates that increasing the accordingly normalised rate $\bar{a}$ implies increasing values of $\hat{D}$. Here the definition $\bar{a} = (a/\kappa)\ln Re$ reflects the classical small-defect scaling. In other words, for any fixed Reynolds number the lowest and highest values of $\hat{D}$ correspond to, respectively, the minimum $\bar{a}_{min}$ and the maximum $\bar{a}_{max}$ of $\bar{a}$ considered in the numerical computations. In the cases presented here $\bar{a}_{min} = 1.0$ and $\bar{a}_{max} = 4.5$. (It is noted that in Fig. 5 (a) only the parts of the curves corresponding to values of $\bar{a}$ such that $\hat{D} > 0.5$ are visible.) The resulting curves are qualitatively in good agreement with the predictions of the asymptotic analysis, where $a \sim \varepsilon\Sigma_1$ with Σ_1 given by (64) and the Reynolds number enters in the form $1/\ln Re$. For $m+1/3$ sufficiently close to 0_+, the limit (64b) applies. Hence, in the double limit (1) and (56) the collapse of the numerical results for incrementally ascending values of $\lg Re$ onto the canonical relationship (74) expected in the limit $Re \to \infty$ is rather slow apparently. This observation substantiates the conclusions already drawn from the discrepancy between asymptotic and experimental results in connection with Figs. 3. As an equally important influence on this decreasing deviation of the numerical results for consecutive values of Re, however, the logarithmic singularity, see (79b), increasingly imposes numerical difficulties and thus impairs their accuracy.

For the time being, a thorough comparison between numerical and measured data is hampered by the fact that samples of the latter which satisfy the necessary requirements of the underlying theory sufficiently well are scarce. Nonetheless, an attempt has been made by representing quasi-equilibrium through the dependence of the shape factor G on m. To this end, the measurements by Simpson et al. [58] presented in [6] were adopted, who considered a flow approaching separation where m varies slowly in the streamwise direction for $Re \approx 3 \times 10^6$. Although this flow configuration causes deviations from equilibrium which allowedly renders the use of the notion quasi-equilibrium at least questionable, the experimental data exhibit the same qualitative behaviour as the numerical results, see Fig. 5 (b), again in support of the theoretical considerations. It is furthermore mentioned that, according to (65) and (72), the minimum values of μ satisfy the asymptotic relationship

$$\varepsilon r \sim 6\mu, \tag{86}$$

which is obtained by neglecting effects due to surface curvature and Reynolds normal stresses: see (75b). This behaviour is in satisfactory agreement with the semi-empirical result

$$\varepsilon G \approx 5\mu, \tag{87}$$

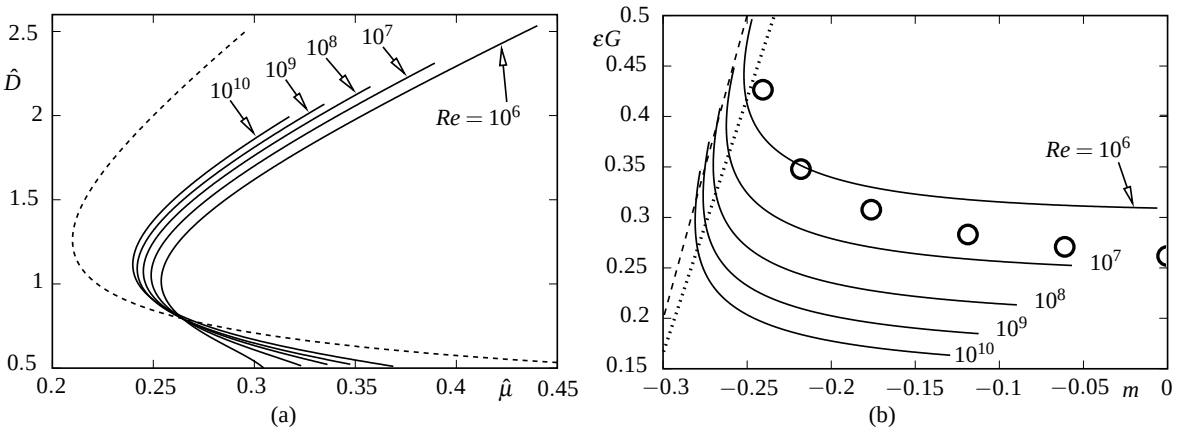

Fig. 5 Comparison of numerical results (*solid*) with (a) the canonical relationship (74) (*dashed*), (b) experimental data by [58] (O, taken from [6]) and relationships (86) (*dashed*) and (87) (*dotted*)

proposed by Härtl [59] (see also [6], p. 590). As mentioned above, the lower branches in Figs. 5 correspond to the small-defect results, recovered for $\hat{\mu} \to \infty$. The dotted curves in Fig. 4 (b) were also obtained from these numerical computations. They confirm the aforementioned slow convergence for $Re \to \infty$, whereas the disagreement with the solid ones satisfying (75a) for $\lg Re = 6$ and 10 is due to higher-order effects not resolved by the present theory.

Finally, the velocity defect profiles for the same values of Re as in Figs. 5 and the aforementioned minimum and maximum values of $\bar{a}$ are plotted in Figs. 6. As mentioned in this context and expected from the asymptotic analysis in Sect. 3, the collapse of the solutions for the upper limit $\bar{a}_{max}$ of $\bar{a}$ which, therefore, exhibit a moderately large velocity defect, is rather slow. However, by applying the transformation (83) and (84), giving $(1-f')/\gamma = \beta^{1/2}F'$, they nevertheless qualitatively resemble the wake-type shape predicted by the present theory in the limit $\varepsilon \to 0$ as shown by the canonical representation in Fig. 3 (b). Specifically, the regime of the intermediate layer which accounts for the transition of the outer wake-like towards the logarithmic portions of the velocity profiles is clearly visible. Also, both the sets of curves for the lower/higher value of $\bar{a}$ are seen to excellently confirm the classical (small-defect)/non-classical (moderately-large-defect) scaling laws. In particular, the results displayed in Fig. 6 (b) confirm that $t \sim 1$ as $\eta \to 0$, and the curves in Figs. 6 (c, d) unambiguously reproduce the asymptotic defect and shear stress distributions shown in Fig. 3 (b) with sufficient accuracy given the values of Re available here.

5 Concluding remarks and further outlook

A comprehensive theory of wall-bounded turbulent boundary layers based upon passage to the limit given by (1) is established. The powerful method of matched asymptotic expansions undeniably provides the proper tool to cope with the principal intricacies arising from the unclosed Reynolds-averaged equations of motion as we target at not being restrained by a particular closure model. We accomplish this by positing the two basic suppositions commencing this work: it is demonstrated how the classical theory, characterised by an internal two-layer splitting of the boundary layer with an asymptotically small streamwise velocity defect in the outer layer, is essentially traced back to the single Hypothesis 1. This then is generalised in terms of Hypothesis 2. The novel self-consistent flow description founded on the latter extends the classical small-defect approach insofar as the order of magnitude of the velocity defect may become independent of the Reynolds number Re but, however, is considered as small compared to unity. Consequently, in the specific limit (36) utilised the interesting phenomenon of non-unique self-preserving flows for large values of β is confirmed on a profound theoretical basis. In particular, the analysis gives rise in the necessary condition (72) for the existence of equilibrium flows, where the inverse of the similarity parameter Γ introduced by (36) serves as a measure for the wall shear stress. Most interestingly, the procedure can apparently be interpreted as an asymptotically exact integral method. As the strictly positive deviation of the external-flow exponent m from its lower bound given by $m = -1/3$ slightly depends on Re, these flows are seen to withstand the maximum externally imposed pressure rise possible for a given value of Re. From the viewpoint of matched asymptotic expansions, this

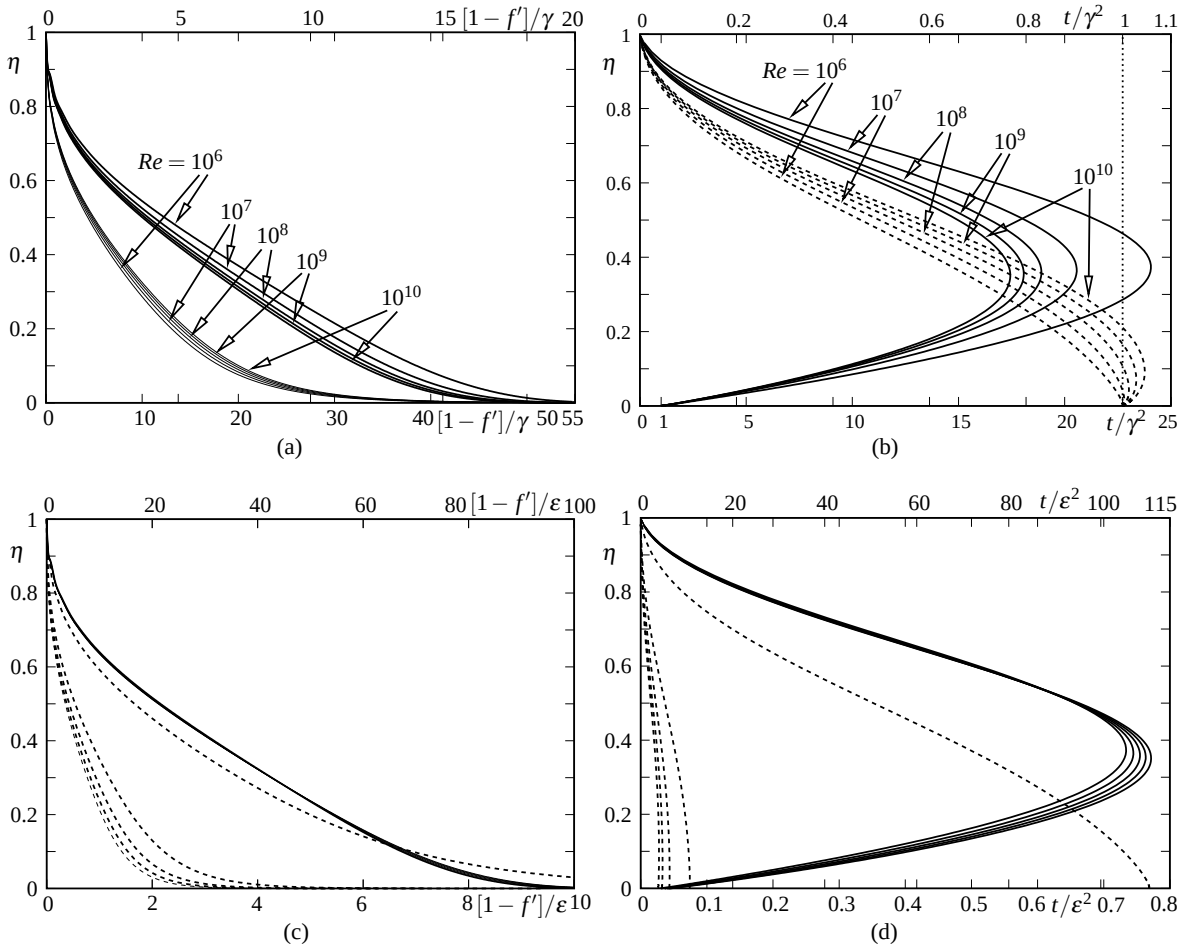

Fig. 6 Distributions for $\bar{a} = \bar{a}_{min} = 1.0$ ((a) *thin solid*, (b–d) *dashed*) and $\bar{a} = \bar{a}_{max} = 4.5$ (*thick solid*) of (a, c) velocity defect, (b, d) Reynolds shear stress, in (a, b) classical, (c, d) non-classical scaling; curves in (c, d) parametrised as in (a, b): maximum abscissa values of top ($\bar{a} = \bar{a}_{min}$) / bottom ($\bar{a} = \bar{a}_{max}$) abscissae increase / decrease for increasing values of *Re*

strikingly contrasts with the conventional hierarchical schemes, where the existence of the external flow is definitely not linked to the specific value of *Re*. Here the resulting two-valued dependences on *Re* controlled by Γ collapse to a single one governed by the canonical relationships (74). These form a universal or similarity law displayed in Fig. 4 (a) and represent a cornerstone of the present analysis.

It is encouraging that the stringent prediction of multi-valued turbulent boundary layers in model-free manner is strongly supported by the well-known early experimental study of near-equilibrium flows by Clauser [41] and even more recent measurements, see Elsberry et al. [55], for instance. Moreover, this issue is also brought up in the semi-theoretical investigation of equilibrium boundary layers by Townsend [35] and by studies adopting semi-empirical integral methods, cf. Winter & East [60], Schlichting & Gersten [6], and Mikhailov [27]. In this context one also should note the calculations put forward by Head [24], which attest the impossibility of attaining equilibrium particularly for $m \doteq -0.35$. From an engineering point of view, the influence of wall percolation or suction/injection on the phenomenon of non-unique equilibrium flows may be of interest in future.

We note that for the surface geometry discussed in connection with (55), exact power-law flows (for $\hat{K} = 0$) can be deemed as also sufficient for achieving (52a) and (52b) if they are consistent with the conditions that arise from matching the turbulent boundary layer flow with that in a state of laminar–turbulent transition in the neighbourhood of the virtual origin. Here we only note the requirement $\delta \to 0$ as $x \to 0_+$, which renders the two-term expansion $\delta/\varepsilon \sim (\Sigma_1 + \varepsilon\Sigma_2)x$ found for second-order equilibrium uniformly valid. At present, this match is confirmed for $m = 1$ by the analysis of boundary layers emanating from a stagnation point by Scheichl et al. [51]; see also [45]. However, an exhaustive analysis of this limiting behaviour, for both the

classical small-defect and the singular moderately-large-defect case, is still unavailable. In particular, the self-similar forms of the first- and second-order boundary layer equations and the effect of the pressure gradient on the equilibrium in the viscous wall layer as $x \to 0_+$, both possibly associated with a further breakdown near the virtual origin, still require clarification. One might associate this scenario with a splitting of the wall layer in streamwise direction as the classical equilibrium hierarchy expressed by (16) ceases due to the inevitable growth of $\delta_n u$ and p^+ since $u_\nu = u_\tau = O(x\gamma)$, see (11). As a result of this shortening of the streamwise scale, the logarithmic overlap law, provided by (17), would atypically be accompanied by a linear variation of the shear stress with distance from the wall. As shown in [45], however, both the outer small-defect structure, tied in with (17), and the conventional leading-order equilibrium between wall shear and total stress in the wall region, apart from a thin sublayer, stay intact even under action of an imposed unbounded pressure gradient that finally provokes massive separation. This finding is potentially of interest for a deepened analysis of the boundary layer origin.

Open demanding questions already raised in [41] include, among others, the existence of flows connecting two equilibrium solutions as indicated in Fig. 3 (b) associated with a hysteresis, also in connection with unsteady effects, and the possibility to extend the present theory to velocity defects of $O(1)$. We emphasise that it was already argued in [41] and [35] that the lower branch characterised by the relatively smaller velocity defect is temporally stable, and these observations were also validated preliminarily by the unsteady asymptotic analysis addressed by Scheichl & Kluwick [18]. In addition, increased efforts in studying the behaviour of non-unique near-equilibrium turbulent boundary layers experimentally, and, if possible, by means of Direct Numerical and/or Large-Eddy Simulation seem desirable.

Finally but vitally important, tackling the extremely challenging task of substantiating the basic Hypothesis 2 by arguments which are derived from first principles seems of utmost importance in itself. However, the insight gained would be of great value also for the progress in the development of a most general rational theory of turbulent boundary layers which includes the possibility of a large velocity defect. Although the direction investigated by Scheichl [57], see also Kluwick & Scheichl [11], has proven promising, even more should be done to underpin the asymptotic structure of large-defect flows.

Acknowledgements This research was supported partly by the Austrian Science Fund (FWF, project no.: P16555-N12) and partly by the Austrian Research Promotion Agency (FFG) within the Austrian Competence Centers for Excellent Technologies (COMET) K2 Programme (project no.: 824187, project acronym: XTribology). Cambridge University Press is greatly acknowledged for granting approval to the reproduction of the data in Figs. 3 (a), (c), (d), published originally by Skåre & Krogstad [36].

A Appendix: Further aspects of the second-order analysis

In the following we highlight some mathematical details, in order to to state the (necessary and sufficient) prerequisites for non-unique flows in a more precise manner.

A.1 Prerequisites underlying prediction of non-uniqueness

At first, we emphasise that the requirements (65) for the external flow remarkably follow directly from three properties which essentially determine the elucidated asymptotic structure of the flow in the outermost core regime of the boundary layer:

$$\text{(I)}\ \ 1-u/U_e \sim \varepsilon \hat{F}'(\eta), \quad \text{(II)}\ \ -\langle u'v'\rangle/U_e^2 \sim \varepsilon^2 \hat{T}(\eta), \quad \text{(III)}\ \ \hat{F}(0)=\hat{T}(0)=0. \tag{A 1}$$

Herein items (I) and (II) rely on (6a) and (6b), respectively. Also, they are equivalent to an asymptotically constant value of ℓ/y, akin to (20), holding inside the intermediate layer by matching. Specifically, they imply homogeneous matching conditions for the universal leading-order results as expressed by (III). As pointed out earlier, the resulting overlap with the near-wall flow regions resembling the behaviour of a wake near its centreline not only has a sound experimental but, most important, also theoretical basis as it is purely a consequence of Hypothesis 2.

A.2 Solvability criterion in a formal perspective

Secondly, the question arises inevitably whether the necessary conditions listed at the beginning of Subsect. 3.3.3 are sufficient for the existence of a solution, comprising $[\bar{F}_2, T_2](\eta)$ and Σ_2, of the second-order problem 76a, 76b. In mathematical terms, we ask for the existence of $\bar{F}_2$, in order that the relationship determining the eigenvalue Σ_2 are satisfied, namely (69) giving (71a) and the solvability condition (72) giving (71b) and predicting non-uniqueness for $\sigma = 0$. This raises the question whether the

solvability of the second-order problem is seen as a justification or even selection of asymptotically correct turbulence models, which poses an intriguing though prohibitively formidable task. For the time being, we can "answer this question" only by closing T_2 in terms of an algebraic turbulence model, though even then not conclusively in the classical case (64a). However, we tentatively expect that the results are also of interest in a much wider context. We exemplify this attempt by adopting the mixing-length closure at hand, which yields (76c) and thereby completes the Sturm–Liouville boundary value problem (76) for $\bar{F}_2(\eta)$. This is singular for both $\eta = 0$ and $\eta = 1$, since l^2F_1'' is of $O\big(\eta^{(1+\sigma)/2)}\big)$ as $\eta \to 0_+$ and of $O(n)$ as $n = 1-\eta \to 0_+$, where we refer to (42), (59), and Figs. 3 (a–c). More precisely, we have $l(1) > 0$ and $F_1 \sim -F_1'''(1)\,n^3/6$ in the last limit, with $F_1'''(1) > 0$.

Regarding the case (64a), let $\bar{F}_{2h}(\eta)$ satisfy the homogeneous form

$$\Sigma_1\big[(m+1)\eta\,\mathrm{d}/\mathrm{d}\eta - 3m - 1\big]\bar{F}_{2h} = 2l^2F_1''\bar{F}_{2h}'' \tag{A 2}$$

of (76), subject to the homogeneous boundary conditions expressed by (76b). Denote by $[H_1,H_2](\eta;m)$ a singular and a regular fundamental solution of (A 2) with $H_1 \sim 1+O(\eta\ln\eta)$ and $H_2 \sim \eta + O(\eta^2)$ as $\eta \to 0_+$, where we dismiss H_1 on grounds of (76b). One then constructs another set of two linearly independent solutions, having the in general irregular and regular asymptotic representations $n^a + O(n^{a+1})$ with $a = 1+(1+m)/[2l(1)^2F_1'''(1)] > 1$ and $1 - n(3m+1)/(m+1) + O(n^2)$ as $n \to 0_+$. Consequently, here the second candidate has to be discarded. Furthermore, for any distribution $l(\eta)$ (referring to a specific customary algebraic closure) the situation of straight proportionality between both admissible solutions can tolerably be regarded as over-restrictive, i.e. very unlikely if not spurious. In turn, the first/second remaining solution is composed non-trivially of both members of the first/second fundamental basis and is hence rejected. But then $\bar{F}_{2h} \equiv 0$, which finally entails existence and uniqueness of the second-order solution $\bar{F}_2(\eta)$ satisfying (76), without the need of further restrictions on the inhomogeneity ρ, i.e. on the first-order solution $F_1(\eta)$. For the sake of completeness, we note that H_1 and H_2 interdepend as e.g.

$$H_2 = \int_0^\eta \frac{\mathrm{d}\bar{\eta}}{(H_1^2\Lambda)(\bar{\eta};m)}, \quad \text{with} \quad \Lambda(\eta;m) = \exp\int_\eta^0 \frac{\Sigma_1(m+1)\bar{\eta}}{2(l^2\hat{F}'')(\bar{\eta})}\,\mathrm{d}\bar{\eta} \tag{A 3}$$

being the inverse of their Wronskian. We then give the solution of the second-order problem (76) in the form

$$\bar{F}_2 = \left[H_2\int_1^\eta H_1(\bar{\eta}) - H_1\int_0^\eta H_2(\bar{\eta})\right]\Big(\Sigma_1\rho(\bar{\eta};m,\hat{K}) + \Sigma_2\big[(m+1)\eta\,\mathrm{d}/\mathrm{d}\eta - 3m - 1\big]F_1\Big)\frac{\Lambda(\bar{\eta};m)}{2(l^2F_1'')(\bar{\eta})}\,\mathrm{d}\bar{\eta}. \tag{A 4}$$

The existence of the integrals in (A 3) and (A 4) is guaranteed by the above estimates holding in the limit $n \to 0_+$ and the fact that the inhomogeneity in (76a), set in parentheses in (A 4), vanishes as $\eta \to 0$: see (66a). Although the circumstance of a non-trivial $\bar{F}_{2h}$ is rarely expected and likewise uncommon, rounding off the considerations above with a rigorous proof is still missing. Notwithstanding, if (76) represents a Fredholm operator acting on $\bar{F}_2$, one can dispense with this difficulty safely by considering the solution $\bar{F}_{2h}^\dagger(\eta)$ of the adjoint homogeneous problem

$$\Sigma_1\big[(m+1)(\eta\bar{F}_{2h}^\dagger)' + (3m+1)\bar{F}_{2h}^\dagger\big] + 2(l^2F_1''\bar{F}_{2h}^\dagger)'' = 0, \tag{A 5a}$$

$$\bar{F}_{2h}^\dagger(0) = \bar{F}_{2h}^\dagger(1) = 0. \tag{A 5b}$$

This is obtained by invoking (76b) and the aforementioned small-η behaviour of F_1'' and l and integration by parts in standard manner. Two fundamental solutions of (A 5a) exhibit the regular and irregular behaviour $1+O(\eta)$ and $1/\eta + O(\ln\eta)$, respectively, as $\eta \to 0$. Then $\bar{F}_{2h}^\dagger \equiv 0$ and $\bar{F}_{2h} \equiv 0$ too, so that the existence of a unique $\bar{F}_2$ ensues from applying Fredholm's alternative to (76).

The transition of (A 4) towards (77c) in the special case (64b) governing a moderately large defect now follows from the relationship $\Lambda(\eta;-1/3) = (W_1/F_1')^{1/2}$, which we derived by adopting (58). However, here the explicit solution (77c) of (76) settles the introductory question: non-uniqueness arises from (72) solely, to wit neither the specific form of the first- nor that of the second-order solution, $\hat{F}(\eta)$ and $\bar{\hat{F}}(\eta)$, respectively.

References

1. Yajnik, K.S.: Asymptotic theory of turbulent shear flows. J. Fluid Mech. **42** (2), 411–427 (1970)
2. Bush, W.B., Fendell, F.E.: Asymptotic analysis of turbulent channel and boundary-layer flow. J. Fluid Mech. **56** (4), 657–681 (1972)
3. Fendell, F.E.: Singular perturbation and turbulent shear flow near walls. J. Astronaut. Sci. **20** (11), 129–165 (1972)
4. Mellor, G.L.: The large Reynolds number, asymptotic theory of turbulent boundary layers. Int. J. Eng. Sci. **10** (10), 851–873 (1972)
5. Walker, J.D.A.: Turbulent Boundary Layers II: Further Developments. In: Kluwick, A. (ed.) Recent Advances in Boundary Layer Theory, CISM Courses and Lectures No. 390, pp. 145–229. Springer, Wien, New York (1998)
6. Schlichting, H., Gersten, K.: Boundary-Layer Theory (8th ed.). Springer, Berlin, Heidelberg, New York (2003)
7. Deriat, E., Guiraud, J.-P.: On the asymptotic description of turbulent boundary layers. J. Theor. Appl. Mech., Special issue: Asymptotic Modelling of Fluid Flows (J. Méc. Théor. Appl., Numéro spécial: Modelisation Asymptotique D'Ecoulements de Fluides), 109–140 (1986)
8. Kolmogorov, A.N.: A refinement of previous hypotheses concerning the local structure of turbulence in a viscous incompressible fluid at high Reynolds number. J. Fluid Mech. **13** (1), 82–85 (1961)

9. Hinze, J.O.: Turbulence. McGraw-Hill, New York (1975)
10. Monin, A.S., Yaglom, A.M.: Statistical Fluid Mechanics: Mechanics of Turbulence. Vol 2. MIT Press, Cambridge (MA), London (1975)
11. Kluwick, A., Scheichl, B.: High-Reynolds-Number Asymptotics of Turbulent Boundary Layers: From Fully Attached to Marginally Separated Flows. In: Hegarty, A., Kopteva, N., ORiordan, E., Stynes, M. (eds.) BAIL 2008 – Boundary and Interior Layers. Proceedings of the International Conference on Boundary and Interior Layers – Computational and Asymptotic Methods, Limerick, July 2008, Lecture Notes in Computational Science and Engineering, Vol. 69, pp. 3–22. Springer, Berlin, Heidelberg (2009)
12. Clauser, F.H.: The turbulent boundary layer. Adv. Appl. Mech. **4**, 1–51 (1956)
13. Van Dyke, M.: Perturbation Methods in Fluid Mechanics (Annotated ed.). Parabolic Press, Stanford (1975)
14. Fraenkel, L.E.: On the method of matched asymptotic expansions. Parts I–III. Proc. Camb. Phil. Soc. **65**, 209–284 (1969).
15. McKeon, B.J., Li, J., Jiang, W., Morrison, J.F., Smits, A.J.: Further observations on the mean velocity distribution in fully developed pipe flow. J. Fluid Mech. **501**, 135–147 (2004)
16. Walker, J.D.A., Abbott, D.E., Scharnhorst, R.K., Weigand, G.G.: Wall-layer model for the velocity profile in turbulent flows. AIAA J. **27** (2), 140–149 (1989)
17. Butler, M.J., Duck, P.W., Stansby, P.K.: An asymptotic description of the attached, turbulent, oscillatory boundary layer. J. Eng. Math. **34** (3), 335–357 (1998)
18. Scheichl, B., Kluwick, A.: Non-Unique Quasi-Equilibrium Turbulent Boundary Layers. In: Gutkowski, W., Kowalewski, T.A. (eds.) 21st Int'l Congress Theor. Appl. Mech. ICTAM04 Abstracts Book and CD-ROM Proceedings, August 15–21, 2004, Warsaw, Poland, 57, Lecture Code FM2L_11083. IPPT PAN, Warsaw (2004)
19. Monin, A.S., Yaglom, A.M.: Statistical Fluid Mechanics: Mechanics of Turbulence. Vol. 1. MIT Press, Cambridge (MA), London (1971)
20. Neish, A., Smith, F.T.: On turbulent separation in the flow past a bluff body. J. Fluid Mech. **241**, 443–467 (1992)
21. Kader, B.A., Yaglom, A.M.: Similarity treatment of moving-equilibrium turbulent boundary layers in adverse pressure gradients. J. Fluid Mech. **89** (2), 305–342 (1978)
22. Mellor, G.L., Gibson, D.M.: Equilibrium turbulent boundary layers. J. Fluid Mech. **24** (2), 225–253 (1966)
23. Mellor, G.L.: The effects of pressure gradient on turbulent flow near a smooth wall. J. Fluid Mech. **24** (2), 255–274 (1966)
24. Head, M.R.: Equilibrium and near-equilibrium turbulent boundary layers. J. Fluid Mech. **73** (1), 1–8 (1976)
25. Schofield, W.H.: Equilibrium boundary layers in moderate to strong adverse pressure gradients. J. Fluid Mech. **113**, 91–122 (1981)
26. Skote, M., Henningson, D.S.: Direct Numerical Simulation of self-similar turbulent boundary layers in adverse pressure gradients. Flow, Turbulence and Combustion **60**, 47–85 (1998)
27. Mikhailov, V.V.: Universal velocity defect law for the turbulent boundary layer. Fluid Dyn. **40** (2), 245–255 (2005), translated from Izv. Ross. Acad. Nauk, Mekh. Zhidk. i Gaza **2**, 89–101 (2005)
28. Melnik, R.E.: An asymptotic theory of turbulent separation. Computers & Fluids **17** (1), 165–184 (1989)
29. Sychev, V.V., Sychev, Vik. V.: On turbulent boundary layer structure. PMM U.S.S.R. **51** (4), 462–467 (1987), translated from Prikl. Matem. Mekhan. **51** (4), 593–599 (1987)
30. Afzal, N.: Wake layer in a turbulent boundary layer: a new approach. In: Gersten, K. (ed.) Proc. IUTAM Symposium on Asymptotic Methods for Turbulent Shear Flows at High Reynolds Numbers, Bochum, Germany, June 28–30, 1995, Fluid Mechanics and Its Applications, Vol. 37, pp. 95–118. Kluwer Academic, Dordrecht (NL), Boston, London (1995)
31. Afzal, N.: Analysis of a turbulent boundary layer subjected to a strong pressure gradient. Int. J. Eng. Sci. **21** (6), 563–576 (1983)
32. George, W.K.: Some New Ideas for Similarity of Turbulent Shear Flows. In: Hanjalić, K., Pereira, J.C.F. (eds.) Turbulence, Heat and Mass Transfer, Vol. 1, pp. 13–24. Begell House, New York, Wallingford (GB) (1995)
33. George, W.K., Castillo, L.: Zero-pressure-gradient turbulent boundary layer. Appl. Mech. Rev. **50** (12), Part 1, 689–729 (2001)
34. Castillo, L., George, W.K.: Similarity analysis for turbulent boundary layer with pressure gradient: outer flow. AIAA J. **39** (1), 41–47 (2001)
35. Townsend, A.A.: Equilibrium layers and wall turbulence. J. Fluid Mech. **11** (1), 97–120 (1961)
36. Skåre, P.E., Krogstad, P.-Å.: A turbulent equilibrium boundary layer near separation. J. Fluid Mech. **272**, 319–348 (1994)
37. Stratford, B.S.: The prediction of separation of the turbulent boundary layer. J. Fluid Mech. **5** (1), 1–16 (1959)
38. Perry, A.E., Bell, J.B., Joubert, P.N.: Velocity and temperature profiles in adverse pressure gradient turbulent boundary layers. J. Fluid Mech. **25** (2), 299–320 (1966)
39. Perry, A.E., Schofield, W.H.: Mean velocity and shear stress distributions in turbulent boundary layers. Phys. Fluids **16** (12), 2068–2074 (1973)
40. Jeken, B.: Asymptotic analysis of turbulent boundary layers at curved walls using a Reynolds stress model. ZAMM — Z. angew. Math. Mech. **72** (5), T308–T312 (1992)
41. Clauser, F.H.: Turbulent boundary layers in adverse pressure gradients. J. Aeronaut. Sci. **21** (2), 91–108 (1954)
42. Scheichl, B., Kluwick, A.: Non-Unique Self-Similar Turbulent Boundary Layers in the Limit of Large Reynolds Number. In: Peinke, J., Kittel, A., Barth, S., Oberlack, M. (eds.) Progress in Turbulence, Springer Proceedings in Physics, Vol. 101, pp. 111–116. Springer, Berlin, Heidelberg, New York (2005)
43. Smith, F.T., Merkin, J.H.: Triple-deck solutions for subsonic flows past humps, steps, concave or convex corners and wedged trailing edges. Computers & Fluids **10** (1), 7–25 (1982)
44. Sychev, V.V., Ruban, A.I., Sychev, Vic. V., Korolev, G.L.: Asymptotic Theory of Separated Flows (eds. Messiter, A.F., Van Dyke, M.). Cambridge University Press, Cambridge (1998)
45. Scheichl, B., Kluwick, A., Smith, F.T.: Break-away separation for high turbulence intensity and large Reynolds number. J. Fluid Mech. **670**, 260–300 (2011)
46. Henkes, R.A.W.M.: Scaling of equilibrium boundary layers under adverse pressure gradient using turbulence models. AIAA J. **36** (3), 320–326 (1998)

47. Michel, R., Quémard, C., Durant, R.: Hypothesis on the mixing length and application to the calculation of the turbulent boundary layers. In: Kline, S.J., Morkovin, M.V., Sovran, G., Cockrell, D.J. (eds.) Proc. Computation of Turbulent Boundary Layers – 1968 AFOSR-IFP-Stanford Conference. Vol. I, Stanford, August 19–24, 1968, pp. 195–207. Stanford University, Stanford (1969)
48. Klebanoff, P.S.: Characteristics of turbulence in a boundary layer with zero pressure gradient. NACA-R-1247 (1955), also: NACA-TN-3178 (1954)
49. Granville, P.S.: A modified van Driest formula for the mixing length of turbulent boundary layers in pressure gradients. J. Fluids Eng. **111** (1), 94–97 (1989)
50. Stratford, B.S.: An experimental flow with zero skin friction throughout its region of pressure rise. J. Fluid Mech. **5** (1), 17–35 (1959)
51. Scheichl, B., Kluwick, A., Alletto, M.: "How turbulent" is the boundary layer separating from a bluff body for arbitrarily large Reynolds numbers? Acta Mech. **201** (1–4), 131–151 (2008).
52. Lim, S., Choi, H.: Optimal shape design of a two-dimensional asymmetric diffuser in turbulent flow. AIAA J. **42** (6), 1154–1169 (2004)
53. Meroney, R.N., Bradshaw, P.: Turbulent boundary-layer growth over a longitudinally curved surface. AIAA J. **13** (11), 1448–1453 (1975)
54. Ramaprian, B.R., Shivaprasad, B.G.: Mean flow measurements in turbulent boundary layers along mildly curved surfaces. AIAA J. **15** (2), 189–196 (1977)
55. Elsberry, K., Loeffler, J., Zhou, M.D., Wygnanski, I.: An experimental study of a boundary layer that is maintained on the verge of separation. J. Fluid Mech. **423**, 227–261 (2000)
56. Durbin, P.A., Belcher, S.E.: Scaling of adverse-pressure-gradient turbulent boundary layers. J. Fluid Mech. **238**, 699–722 (1992)
57. Scheichl, B.: Asymptotic Theory of Marginal Turbulent Separation, Doctoral thesis, Vienna University of Technology, Vienna (2001)
58. Simpson, R.L., Chew, Y-T., Shivaprasad, B.G.: The structure of a separating boundary layer. Part 1. Mean flow and Reynolds stresses. J. Fluid Mech. **113**, 23–51 (1981)
59. Härtl, A.P.: Optimierung von Diffusoren durch Konturierung der Wände auf Basis des Grenzschichtkonzeptes. Doctoral thesis, Ruhr-Universität Bochum, Bochum (1989), also: Fortschr.-Ber. VDI Reihe 7, No. 159, VDI-Verlag, Düsseldorf (1989)
60. Winter, K.G., East, L.F.: The Design of Optimum Diffusers for Incompressible Flow. In: Haase, W. (ed.) Recent Contributions to Fluid Mechanics, pp. 312–320. Springer, Berlin Heidelberg N.Y. (1982)